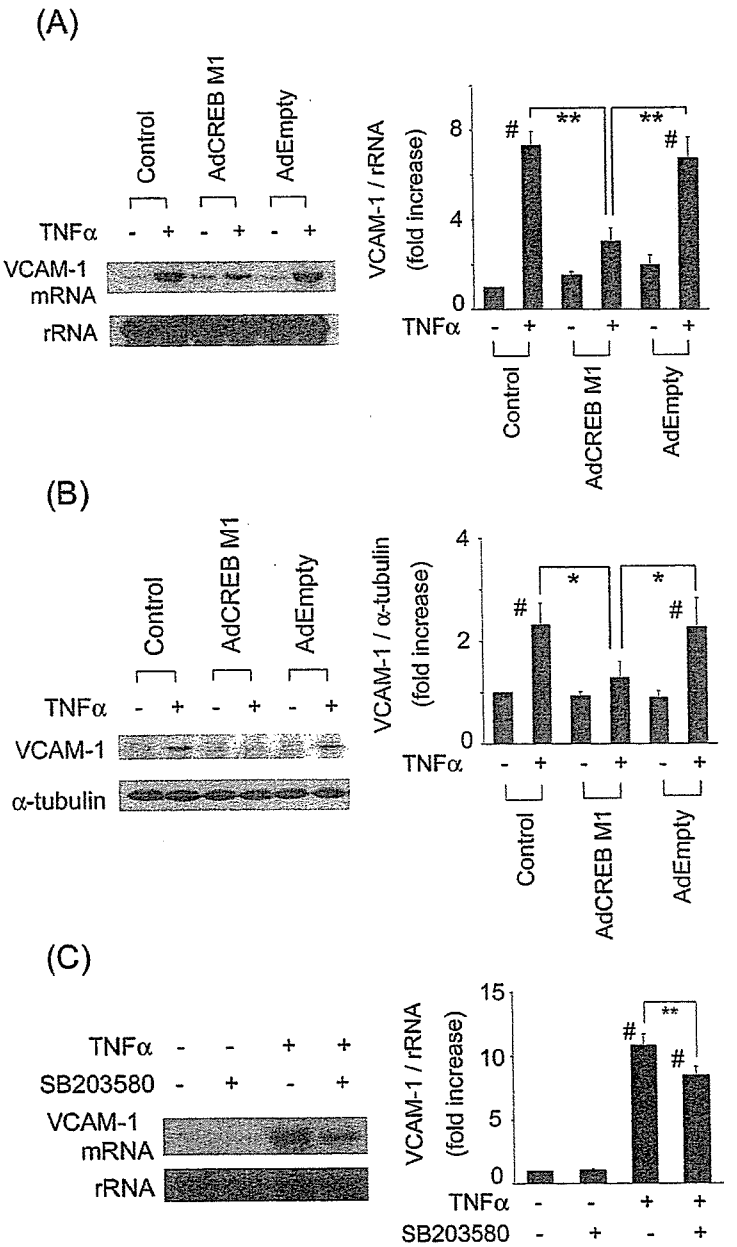

Fig. 4. *AdCREB M1 inhibits TNFα-induced VCAM-1 mRNA and protein expression. A: Bovine ECs were infected with AdCREB M1 (30 MOI) or AdEmpty (30 MOI) and stimulated with or without TNFα (1 ng/ml) for 4 h. TNFα-induced VCAM-1 mRNA expression was detected by Northern blot analysis and the radioactivities of the bands were measured with an imaging analyzer (*n = *4). The radioactivity of VCAM-1 mRNA in TNFα-stimulated cells was normalized against that of rRNA and shown as the relative fold increase compared with that in unstimulated cell. B: Bovine ECs were infected with AdCREB M1 (30 MOI) or AdEmpty (30 MOI) and stimulated with or without TNFα (1 ng/ml) for 12 h. TNFα-induced VCAM-1 protein expression was detected by Western blot analysis (*n = *4) and the ratio of VCAM-1 expression to α-tubulin in TNFα-stimulated cells is shown in the right panel as the relative fold increase compared with that in unstimulated cells. C: Bovine ECs were preincubated with SB203580 (10 μmol/l) for 30 min and stimulated with TNFα (1 ng/ml) for 4 h. TNFα-induced VCAM-1 mRNA expression was detected by Northern blot. The values are expressed as the mean±SEM.* $^{**}p < 0.01$ vs. *AdCREB M1 TNFα (+) or TNFα,* $^{*}p < 0.05$ vs. *AdCREB M1 TNFα (+),* $^{\#}p < 0.01$ vs. *control TNFα (–) or AdEmpty TNFα (–).*

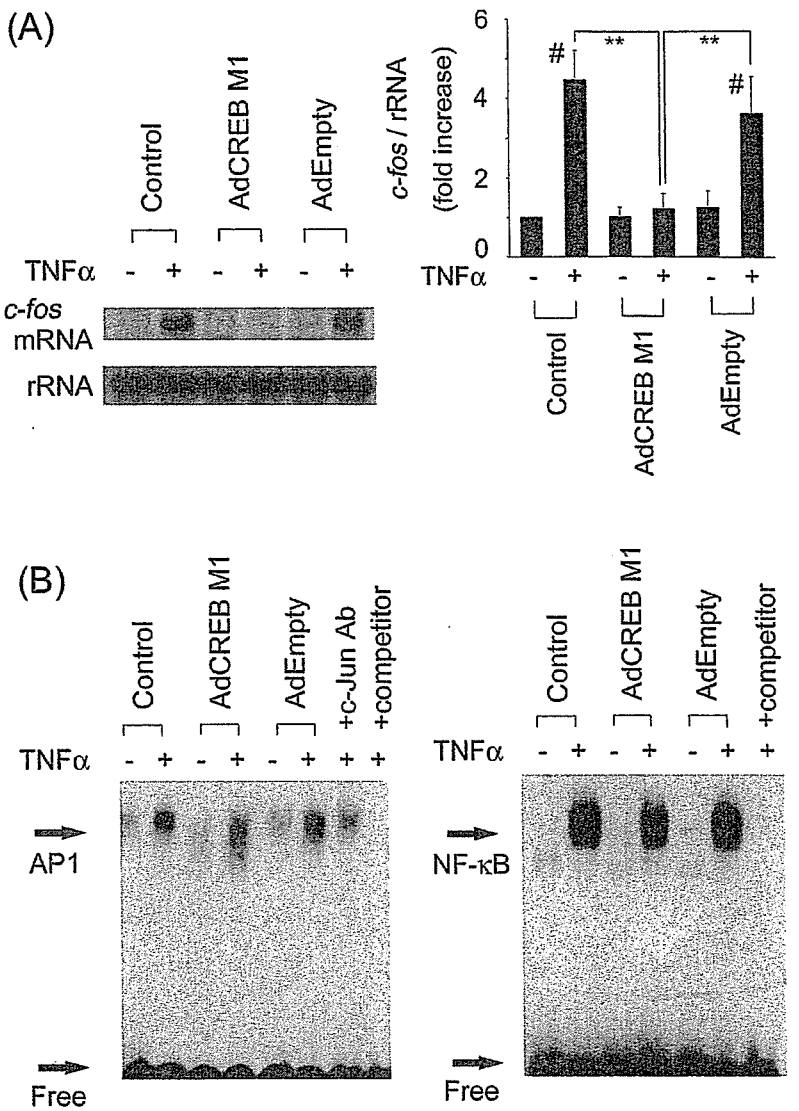

Fig. 5. *AdCREB M1 inhibits TNFα-induced* c-fos *mRNA expression and AP-1 DNA binding activity. A: Bovine ECs were infected with AdCREB M1 (30 MOI) or AdEmpty (30 MOI) and stimulated with or without TNFα (1 ng/ml) for 30 min. TNFα-induced* c-fos *mRNA expression was detected by Northern blot analysis and the radioactivities of the bands were measured with an imaging analyzer* (n=4). *The radioactivity of* c-fos *mRNA was normalized against that of rRNA. The ratio in TNFα-stimulated cells is shown as the relative fold increase compared with that in unstimulated cells. The values are expressed as the mean±SEM.* $^{**}p<0.01$ vs. *AdCREB M1 TNFα (+),* $^{\#}p<0.01$ vs. *control TNFα (−) or AdEmpty TNFα (−). B: Bovine ECs were infected with AdCREB M1 (30 MOI) or AdEmpty (30 MOI) and stimulated with or without TNFα (1 ng/ml) for 4 h. Nuclear extracts were prepared and incubated with radiolabeled AP-1 (left panel) or NF-κB (right panel) probe for 30 min and electrophoresed. A fifty-fold molar excess of unlabeled probe was used as a competitor. For the supershift assay, an antibody against c-Jun was added to the binding reaction mixtures. The same results were obtained in other independent experiments and a representative autoradiogram is shown* (n=4).

gels were dried and exposed to X-ray films.

Statistical Analysis

Statistical analysis was performed with 1-way ANOVA and Fisher's test if appropriate. Values of $p<0.05$ were considered to indicate statistical significance. Data are shown as the mean±SEM.

Results

Phosphorylation of CREB at Ser133 by TNFα

To examine whether CREB is phosphorylated in response to TNFα, we performed Western blot analysis using an antibody that only recognizes the phosphorylated form of CREB at Ser133 (p-CREB). TNFα stimulated phosphorylation of CREB with a peak at 15 min of stimulation (Fig. 1A). TNFα dose-dependently increased phosphorylation of CREB at 15 min of stimulation (Fig. 1B).

The p38-MAPK Pathway Mediates TNFα-Induced CREB Phosphorylation

Several protein kinases are reported to phosphorylate CREB. We examined which pathway is responsible for TNFα-induced CREB phosphorylation. SB203580 (10 μmol/l), a p38-MAPK inhibitor, completely blocked TNFα-induced CREB phosphorylation (Fig. 2A). PD98059 (10 μmol/l), an ERK kinase (MEK) inhibitor, wortmannin (50 nmol/l), an inhibitor of PI3-K, KN93 (10 μmol/l), an inhibitor of CAMKII, and H89 (1 μmol/l), an inhibitor of PKA, did not affect TNFα-induced CREB phosphorylation (Fig. 2A). SP600125, a *c-jun* N-terminal kinase inhibitor, also had no effect on TNFα-induced CREB phosphorylation (data not shown). SB203580 was first described as an inhibitor of p38-MAPK activity that acts by competing with ATP for binding; however, it was later demonstrated that SB203580 also prevents p38-MAPK phosphorylation/activation (*24–26*). SB203580 dose-dependently inhibited TNFα-induced CREB and p38-MAPK phosphorylation (Fig. 2B). To confirm the role of p38-MAPK, we used another p38-MAPK inhibitor, FR167653. FR167653 dose-dependently inhibited TNFα-induced CREB and p38-MAPK phosphorylation (Fig. 2C). TNFα stimulated phosphorylation of p38-MAPK with a peak at 5 min of stimulation, which is faster than phosphorylation of CREB (Fig. 2D). PD98059 and wortmannin at the same concentrations used in Fig. 2 inhibited TNFα-induced ERK and Akt (a target molecule of PI3-K) activation, respectively (data not shown). KN93 and H89 at the same concentrations also inhibited ionomycin- and forskolin-induced CREB phosphorylation, respectively (data not shown). Therefore, the concentrations of these protein kinase inhibitors were sufficient. These data suggest that the p38-MAPK pathway is critical for TNFα-induced CREB phosphorylation.

Overexpression of a Dominant Negative Form of CREB Inhibits TNFα-Induced VCAM-1 Expression

To clarify the role of CREB in the TNFα signaling, we overexpressed a dominant negative form of CREB by an adenovirus vector (AdCREB M1). We used AdEmpty as a negative control for the infection of adenovirus. Phosphorylation of CREB by TNFα was attenuated by infection of AdCREB M1, but not by AdEmpty (Fig. 3). A previous study demonstrated that TNFα stimulated VCAM-1 expression in ECs (*11*). In the present study, AdCREB M1 but not AdEmpty suppressed TNFα-induced VCAM-1 mRNA and protein expression (Fig. 4A, B). SB203580 also suppressed TNFα-induced VCAM-1 mRNA expression (Fig. 4C), suggesting that the p38-MAPK/CREB pathway plays an important role. It is known that TNFα induces VCAM-1 expression through activation of NF-κB and AP-1 (*27*). AP-1 is a heterodimer of c-Fos and c-Jun and CRE is one of the important *cis*-DNA elements regulating *c-fos* gene expression. We therefore hypothesized that dominant negative CREB may affect *c-fos* induction and AP-1 activation. AdCREB M1 but not AdEmpty suppressed TNFα-induced *c-fos* mRNA expression (Fig. 5A). Furthermore, AdCREB M1 suppressed AP-1 DNA binding activity to the consensus sequence induced by TNFα, but it did not affect NF-κB binding activity (Fig. 5B). The binding of AP-1 was specific because the band was eliminated by a 50 mol excess of unlabeled competitor, and the band was supershifted by addition of an antibody against c-Jun. These data suggest that AdCREB M1 may suppress TNFα-induced VCAM-1 gene expression through inhibition of not only CREB but also AP-1 activity.

Discussion

In the present study, we showed that TNFα activated CREB through p38-MAPK. Inhibition of CREB function by a dominant negative molecule suppressed TNFα-induced AP-1 activity and VCAM-1 expression.

The results of a search for *cis*-DNA elements of the VCAM-1 gene promoter by TFSEACH showed the presence of a possible CRE site in the promoter of VCAM-1 at −1686 bp. Therefore, our result suggests that the CRE site of the VCAM-1 gene promoter may play an important role in VCAM-1 expression induced by TNFα. A previous study demonstrated that TNFα stimulated VCAM-1 expression through two NF-κB sites (present at −63 bp and −77 bp from the transcription initiation site) (*11*). Ahmad *et al.* reported that the AP-1/NF-κB complex was induced by TNFα and regulated VCAM-1 gene expression (*27*). AP-1 can interact with other transcription factors and modulate their transcriptional activity (*28*).The p65 subunit of NF-κB requires a co-factor protein for transcriptional activity and can interact with c-Fos and c-Jun through the Rel homology domain (*29*). CRE in the promoter region of the *c-fos* gene plays an important role in the induction of *c-fos* by many stimuli (*30–32*). We confirmed that CRE mediates *c-fos* expression by TNFα. These data suggest that inhibition of AP-1 activity by AdCREB M1 may be involved in the suppression of TNFα-induced VCAM-1 expression. However, further study is necessary to confirm the role of the AP-1 site of the VCAM-1 gene promoter in response to TNFα.

TNFα is known to activate the mitogen-activated protein kinases (MAPKs), such as *c-jun* NH_2-terminal kinase and p38-MAPK in ECs (*33*, *34*). A previous study demonstrated that p38-MAPK mediated actin filament reorganization by several stimuli, such as vascular endothelial growth factor or oxidative stress, in human umbilical vein ECs (*35*). Another study demonstrated that p38-MAPK negatively regulated cell survival and proliferation by FGF-2 stimulation in bovine capillary ECs (*36*). In the present study, we demonstrated that p38-MAPK mediated TNFα-induced CREB phosphorylation and could modulate the expression of cytoadhesion molecules. The p38-MAPK family includes four isoforms, p38α, p38β, p38γ and p38δ. Vascular EC expresses p38α, p38β and p38δ (*37*). SB203580 inhibits p38α and p38β, and thus p38α or p38β may mediate TNFα-induced CREB phosphorylation.

Atherosclerotic lesion progression has been shown to depend on persistent, chronic inflammation in the arterial wall and is characterized by the recruitment of monocytes and lymphocytes to the arterial wall (*38*). Adhesion molecules and chemotactic factors mediate the entry of the leukocytes into the subendothelial space. The first step in adhesion, the rolling of leukocytes along the endothelial surface, is mediated by selectins which bind to carbohydrate ligands on leucocytes (*39*, *40*). The firm adhesion of monocytes and T lymphocytes to endothelium is mediated by VCAM-1 on the endothelium, which interacts with the integrin VLA-4 on monocytes and T lymphocytes (*7*). Therefore, VCAM-1 is assumed to be important for atherosclerogenesis, and knockout strategies have been attempted. Although VCAM-1-null mice die during embryogenesis (*41*), it has been shown that atherosclerotic lesion was reduced that the size of atherosclerotic lesions is reduced in VCAM-1 domain 4-deficient mice (*42*), suggesting that VCAM-1 is indeed an important gene product directly involved in the formation of atherosclerotic lesions.

In the present study, we demonstrated the possible involvement of CREB in TNFα-induced VCAM-1 expression. In addition to TNFα, angiotensin II has been shown to stimulate VCAM-1 expression (*43*, *44*), and we and others previously reported that angiotensin II stimulated phosphorylation of CREB (*32*, *45*). Inhibition of CREB may suppress not only TNFα-induced but also angiotensin II-induced VCAM-1 expression. Furthermore, it was previously reported that high blood pressure activates MAPKs (*46–48*) and that p38-MAPK activation induced by high blood pressure is involved in endothelial dysfunction (*48*). Therefore, inhibition of the p38-MAPK/CREB pathway may attenuate endothelial dysfunction in patients with hypertension. Our data suggest that the p38-MAPK/CREB pathway could be a therapeutic target for the prevention of atherosclerosis.

References

1. Ross R: The pathogenesis of atherosclerosis: a perspective for the 1990s. *Nature* 1993; **362**: 801–809.
2. Blann AD, Tse W, Maxwell SJ, Waite MA: Increased levels of the soluble adhesion molecule E-selectin in essential hypertension. *J Hypertens* 1994; **12**: 925–928.
3. DeSouza CA, Dengel DR, Macko RF, Cox K, Seals DR: Elevated levels of circulating cell adhesion molecules in uncomplicated essential hypertension. *Am J Hypertens* 1997; **10**: 1335–1341.
4. Parissis JT, Venetsanou KF, Mentzikof DG, *et al*: Plasma levels of soluble cellular adhesion molecules in patients with arterial hypertension. Correlations with plasma endothelin-1. *Eur J Intern Med* 2001; **12**: 350–356.
5. Kohara K, Tabara Y, Yamamoto Y, Igase M, Nakura J, Miki T: Genotype-specific association between circulating soluble cellular adhesion molecules and carotid intima-media thickness in community residents: J-SHIPP study. Shimanami Health Promoting Program. *Hypertens Res* 2002; **25**: 31–39.
6. Iiyama K, Hajra L, Iiyama M, *et al*: Patterns of vascular cell adhesion molecule-1 and intercellular adhesion molecule-1 expression in rabbit and mouse atherosclerotic lesions and at sites predisposed to lesion formation. *Circ Res* 1999; **85**: 199–207.
7. Alon R, Kassner PD, Carr MW, Finger EB, Hemler ME, Springer TA: The integrin VLA-4 supports tethering and rolling in flow on VCAM-1. *J Cell Biol* 1995; **128**: 1243–1253.
8. Pober JS, Cotran RS: The role of endothelial cells in inflammation. *Transplantation* 1990; **50**: 537–544.
9. Krasinski K, Spyridopoulos I, Kearney M, Losordo DW: *In vivo* blockade of tumor necrosis factor-alpha accelerates functional endothelial recovery after balloon angioplasty. *Circulation* 2001; **104**: 1754–1756.
10. Berk BC, Abe JI, Min W, Surapisitchat J, Yan C: Endothelial atheroprotective and anti-inflammatory mechanisms. *Ann N Y Acad Sci* 2001; **947**: 93–111.
11. Iademarco MF, McQuillan JJ, Rosen GD, Dean DC: Characterization of the promoter for vascular cell adhesion molecule-1 (VCAM-1). *J Biol Chem* 1992; **267**: 16323–16329.
12. Shaywitz AJ, Greenberg ME: CREB: a stimulus-induced transcription factor activated by a diverse array of extracellular signals. *Annu Rev Biochem* 1999; **68**: 821–861.
13. Mayr B, Montminy M: Transcriptional regulation by the phosphorylation-dependent factor CREB. *Nat Rev Mol Cell Biol* 2001; **2**: 599–609.
14. Sheng M, Thompson MA, Greenberg ME: CREB: a Ca^{2+}-regulated transcription factor phosphorylated by calmodulin-dependent kinases. *Science* 1991; **252**: 1427–1430.
15. Xing J, Ginty DD, Greenberg ME: Coupling of the RAS-MAPK pathway to gene activation by RSK2, a growth factor-regulated CREB kinase. *Science* 1996; **273**: 959–963.
16. Sugawara A, Takeuchi K, Uruno A, Kudo M, Sato K, Ito S: Effects of mitogen-activated protein kinase pathway and co-activator CREP-binding protein on peroxisome proliferator-activated receptor-γ-mediated transcription suppression of angiotensin II type 1 receptor gene. *Hypertens Res* 2003; **26**: 623–628.
17. Tan Y, Rouse J, Zhang A, Cariati S, Cohen P, Comb MJ: FGF and stress regulate CREB and ATF-1 *via* a pathway involving p38 MAP kinase and MAPKAP kinase-2. *EMBO J* 1996; **15**: 4629–4642.

18. Du K, Montminy M: CREB is a regulatory target for the protein kinase Akt/PKB. *J Biol Chem* 1998; **273**: 32377–32379.
19. Baud V, and Karin M: Signal transduction by tumor necrosis factor and its relatives. *Trends Cell Biol* 2001; **11**: 372–377.
20. Chen G, Goeddel DV: TNF-R1 signaling: a beautiful pathway. *Science* 2002; **296**: 1634–1635.
21. Tokunou T, Ichiki T, Takeda K, *et al*: Thrombin induces interleukin-6 expression through the cAMP response element in vascular smooth muscle cells. *Arterioscler Thromb Vasc Biol* 2001; **21**: 1759–1763.
22. Somers JP, DeLoia JA, Zeleznik AJ: Adenovirus-directed expression of a nonphosphorylatable mutant of CREB (cAMP response element-binding protein) adversely affects the survival, but not the differentiation, of rat granulosa cells. *Mol Endocrinol* 1999; **13**: 1364–1372.
23. Funakoshi Y, Ichiki T, Ito K, Takeshita A: Induction of interleukin-6 expression by angiotensin II in rat vascular smooth muscle cells. *Hypertension* 1999; **34**: 118–125.
24. Frantz B, Klatt T, Pang M, *et al*: The activation state of p38 mitogen-activated protein kinase determines the efficiency of ATP competition for pyridinylimidazole inhibitor binding. *Biochemistry* 1998; **37**: 13846–13853.
25. Ryder JW, Fahlman R, Wallberg-Henriksson H, Alessi DR, Krook A, Zierath JR: Effect of contraction on mitogen-activated protein kinase signal transduction in skeletal muscle. Involvement of the mitogen- and stress-activated protein kinase 1. *J Biol Chem* 2000; **275**: 1457–1462.
26. Galan A, Garcia-Bermejo ML, Troyano A, *et al*: Stimulation of p38 mitogen-activated protein kinase is an early regulatory event for the cadmium-induced apoptosis in human promonocytic cells. *J Biol Chem* 2000; **275**: 11418–11424.
27. Ahmad M, Theofanidis P, Medford RM: Role of activating protein-1 in the regulation of the vascular cell adhesion molecule-1 gene expression by tumor necrosis factor-alpha. *J Biol Chem* 1998; **273**: 4616–4621.
28. Chinenov Y, Kerppola TK: Close encounters of many kinds: Fos-Jun interactions that mediate transcription regulatory specificity. *Oncogene* 2001; **20**: 2438–2452.
29. Stein B, Baldwin AS Jr, Ballard DW, Greene WC, Angel P, Herrlich P: Cross-coupling of the NF-kappa B p65 and Fos/Jun transcription factors produces potentiated biological function. *EMBO J* 1993; **12**: 3879–3891.
30. Karin M: The regulation of AP-1 activity by mitogen-activated protein kinases. *J Biol Chem* 1995; **270**: 16483–16486.
31. Ichiki T, Tokunou T, Fukuyama K, Iino N, Masuda S, Takeshita A: Cyclic AMP response element-binding protein mediates reactive oxygen species-induced *c-fos* expression. *Hypertension* 2003; **42**: 177–183.
32. Funakoshi Y, Ichiki T, Takeda K, Tokunou T, Iino N, Takeshita A: Critical role of cAMP-response element-binding protein for angiotensin II-induced hypertrophy of vascular smooth muscle cells. *J Biol Chem* 2002; **277**: 18710–18717.
33. Ichijo H: From receptors to stress-activated MAP kinases. *Oncogene* 1999; **18**: 6087–6093.
34. Kishore R, Luedemann C, Bord E, Goukassian D, Losordo DW: Tumor necrosis factor-mediated E2F1 suppression in endothelial cells: differential requirement of c-Jun N-terminal kinase and p38 mitogen-activated protein kinase signal transduction pathways. *Circ Res* 2003; **93**: 932–940.
35. Rousseau S, Houle F, Landry J, Huot J: p38 MAP kinase activation by vascular endothelial growth factor mediates actin reorganization and cell migration in human endothelial cells. *Oncogene* 1997; **15**: 2169–2177.
36. Matsumoto T, Turesson I, Book M, Gerwins P, Claesson-Welsh L: p38 MAP kinase negatively regulates endothelial cell survival, proliferation, and differentiation in FGF-2-stimulated angiogenesis. *J Cell Biol* 2002; **156**: 149–160.
37. Hale KK, Trollinger D, Rihanek M, Manthey CL: Differential expression and activation of p38 mitogen-activated protein kinase alpha, beta, gamma, and delta in inflammatory cell lineages. *J Immunol* 1999; **162**: 4246–4252.
38. Lusis AJ: Atherosclerosis. *Nature* 2000; **407**: 233–241.
39. Moore KL, Patel KD, Bruehl RE, *et al*: P-selectin glycoprotein ligand-1 mediates rolling of human neutrophils on P-selectin. *J Cell Biol* 1995; **128**: 661–671.
40. Dong ZM, Chapman SM, Brown AA, Frenette PS, Hynes RO, Wagner DD: The combined role of P- and E-selectins in atherosclerosis. *J Clin Invest* 1998; **102**: 145–152.
41. Gurtner GC, Davis V, Li H, McCoy MJ, Sharpe A, Cybulsky MI: Targeted disruption of the murine VCAM1 gene: essential role of VCAM-1 in chorioallantoic fusion and placentation. *Genes Dev* 1995; **9**: 1–14.
42. Cybulsky MI, Iiyama K, Li H, *et al*: A major role for VCAM-1, but not ICAM-1, in early atherosclerosis. *J Clin Invest* 2001; **107**: 1255–1262.
43. Pueyo ME, Gonzalez W, Nicoletti A, Savoie F, Arnal JF, Michel JB: Angiotensin II stimulates endothelial vascular cell adhesion molecule-1 *via* nuclear factor-kappaB activation induced by intracellular oxidative stress. *Arterioscler Thromb Vasc Biol* 2000; **20**: 645–651.
44. Costanzo A, Moretti F, Burgio VL, *et al*: Endothelial activation by angiotensin II through NFkappaB and p38 pathways: involvement of NFkappaB-inducible kinase (NIK), free oxygen radicals, and selective inhibition by aspirin. *J Cell Physiol* 2003; **195**: 402–410.
45. Yoshimoto T, Gochou N, Fukai N, Sugiyama T, Shichiri M, Hirata Y: Adrenomedullin inhibits angiotensin II-induced oxidative stress and gene expression in rat endothelial cells. *Hypertens Res* 2005; **28**: 165–172.
46. Ju H, Behm DJ, Nerurkar S, *et al*: p38 MAPK inhibitors ameliorate target organ damage in hypertension: Part 1. p38 MAPK-dependent endothelial dysfunction and hypertension. *J Pharmacol Exp Ther* 2003; **307**: 932–938.
47. Xu Q, Liu Y, Gorospe M, Udelsman R, Holbrook J: Acute hypertension activates mitogen-activated protein kinases in arterial wall. *J Clin Invest* 1996; **97**: 508–514.
48. Imai G, Satoh T, Kumai T, *et al*: Hypertension accelerates diabetic nephropathy in Wistar fatty rats, a model of type 2 diabetes mellitus, *via* mitogen-activated protein kinase cascades and transforming growth factor-beta1. *Hypertens Res* 2003; **26**: 339–347.

Am J Physiol Heart Circ Physiol 291: H1337–H1344, 2006.
First published April 21, 2006; doi:10.1152/ajpheart.01175.2005.

Blockade of NF-κB improves cardiac function and survival after myocardial infarction

Shunichi Kawano,[1] Toru Kubota,[1] Yoshiya Monden,[1] Takaki Tsutsumi,[1] Takahiro Inoue,[1] Natsumi Kawamura,[1] Hiroyuki Tsutsui,[2] and Kenji Sunagawa[1]

[1]*Department of Cardiovascular Medicine, Kyushu University Graduate School of Medical Sciences, Fukuoka; and*
[2]*Department of Cardiovascular Medicine, Hokkaido University Graduate School of Medicine, Sapporo, Japan*

Submitted 6 November 2005; accepted in final form 12 April 2006

Kawano, Shunichi, Toru Kubota, Yoshiya Monden, Takaki Tsutsumi, Takahiro Inoue, Natsumi Kawamura, Hiroyuki Tsutsui, and Kenji Sunagawa. Blockade of NF-κB improves cardiac function and survival after myocardial infarction. *Am J Physiol Heart Circ Physiol* 291: H1337–H1344, 2006. First published April 21, 2006; doi:10.1152/ajpheart.01175.2005.—NF-κB is a key transcription factor that regulates inflammatory processes. In the present study, we tested the hypothesis that blockade of NF-κB ameliorates cardiac remodeling and failure after myocardial infarction (MI). Knockout mice with targeted disruption of the p50 subunit of NF-κB (KO) were used to block the activation of NF-κB. MI was induced by ligation of the left coronary artery in male KO and age-matched wild-type (WT) mice. NF-κB was activated in noninfarct as well as infarct myocardium in WT + MI mice, while the activity was completely abolished in KO mice. Blockade of NF-κB significantly reduced early ventricular rupture after MI and improved survival by ameliorating congestive heart failure. Echocardiographic and pressure measurements revealed that left ventricular fractional shortening and maximum rate of rise of left ventricular pressure were significantly increased and end-diastolic pressure was significantly decreased in KO + MI mice compared with WT + MI mice. Histological analysis demonstrated significant suppression of myocyte hypertrophy as well as interstitial fibrosis in the noninfarct myocardium of KO + MI mice. Blockade of NF-κB did not ameliorate expression of proinflammatory cytokines in infarct or noninfarct myocardium. In contrast, phosphorylation of c-Jun NH_2-terminal kinase was almost completely abolished in KO + MI mice. The present study demonstrates that targeted disruption of the p50 subunit of NF-κB reduces ventricular rupture as well as improves cardiac function and survival after MI. Blockade of NF-κB might be a new therapeutic strategy to attenuate cardiac remodeling and failure after MI.

cardiac remodeling; inflammation; mitogen-activated protein kinases

NUCLEAR FACTOR-κB (NF-κB) is a key transcription factor that regulates inflammatory processes (1). Recent studies have indicated that NF-κB may play important roles in cardiac hypertrophy and remodeling besides promoting inflammation. First, NF-κB has been shown to be activated in the failing human heart (5, 23), where expression of proinflammatory cytokines is exacerbated (10, 22). Second, in vitro studies have shown that activation of NF-κB is required for hypertrophic growth of cardiomyocytes in response to G protein-coupled receptor agonists, including phenylephrine, endothelin-1, and ANG II (7, 18). Third, recent in vivo studies have demonstrated that blockade of NF-κB ameliorates myocardial hypertrophy in response to aortic banding (12) and chronic infusion of ANG II (9). Finally, blockade of NF-κB improves cardiac function and survival without affecting myocardial inflammation in TNF-α-induced cardiomyopathy (8). Therefore, blockade of NF-κB may be a new therapeutic strategy for heart failure by attenuating myocardial hypertrophy and remodeling.

Myocardial infarction (MI) is a major cause of heart failure in most of the developed countries. NF-κB has been shown to be activated after myocardial ischemia. However, the role of NF-κB in MI remains controversial. Morishita et al. (15) reported that blockade of NF-κB reduced the extent of MI in a rat model of ischemia-reperfusion injury (15), suggesting that activation of NF-κB is cytotoxic in ischemia. The reduction of MI size by NF-κB blockade was also observed in a murine model of ischemia-reperfusion injury (2). In contrast, Misra et al. (14) reported that blockade of NF-κB increased infarct size in a murine model of permanent coronary ligation (14), suggesting that the activation of NF-κB might promote cell survival in MI. Furthermore, no study has investigated the long-term effects of NF-κB blockade on cardiac remodeling and failure late after MI. Therefore, the purpose of the present study was to investigate the role of NF-κB activation in early and late phases of MI using a mouse model of permanent coronary ligation. Mice with targeted disruption of the p50 subunit of NF-κB were used to confer chronic inhibition of NF-κB in vivo (19). The results demonstrated that blockade of NF-κB prevented ventricular rupture early after MI and improved survival by ameliorating cardiac dysfunction in the late phase, suggesting that blockade of NF-κB might be a new therapeutic strategy to attenuate ventricular rupture and remodeling after MI.

MATERIALS AND METHODS

Animal model. Mice with targeted disruption of the p50 subunit of NF-κB (19), backcrossed into the FVB background more than six generations (8, 9), were used to block the activation of NF-κB. These mice were born normally without any major defects. Homoknockout mice (KO) were compared with age- and gender-matched wild-type littermates (WT) in each analysis to minimize the effect of genetic background variation. Male mice at the age of 8–14 wk were used unless mentioned otherwise. We induced MI in both WT and KO mice by ligating the left coronary artery at 2–3 mm from the tip of the left auricle under pentobarbital sodium anesthesia (50 mg/kg ip) as previously reported (20). Sham operation without coronary artery ligation was also performed in WT and KO mice. After the operation, mice were housed under climate-controlled conditions and were provided standard food and water ad libitum. During the study period of 12 wk,

Address for reprint requests and other correspondence: T. Kubota, Dept. of Cardiovascular Medicine, Kyushu Univ. Graduate School of Medical Sciences, 3-1-1 Maidashi, Higashi-ku, Fukuoka 812-8582, Japan (e-mail: kubotat@cardiol.med.kyushu-u.ac.jp).

The costs of publication of this article were defrayed in part by the payment of page charges. The article must therefore be hereby marked "*advertisement*" in accordance with 18 U.S.C. Section 1734 solely to indicate this fact.

cages were inspected daily for animals that had died. All dead mice were examined for the presence of pleural effusion and cardiac rupture as well as MI. The cause of death in each mouse was classified as congestive heart failure when the presence of pleural effusion (serous fluid within the chest wall cavity) and increased lung weight were observed or ventricular rupture when the presence of a blood clot within the pericardial sac was found. This experiment was reviewed and approved by the Committee of the Ethics on Animal Experiment, Kyushu University Graduate School of Medical Sciences and carried out in compliance with the Guideline for Animal Experiment, Kyushu University and the Law (No. 105) and Notification (No. 6) of the Government. The investigation conforms to the *Guide for the Care and Use of Laboratory Animals* published by the National Institutes of Health (NIH Publication No. 85–23, revised 1996).

Electrophoretic mobility shift assay. Activation of NF-κB was evaluated by electrophoretic mobility shift assays (EMSA) according to the manufacturer's instructions (Gel Shift Assay System E3300, Promega, Madison, WI). Nuclear protein was isolated from the myocardium as previously reported (8, 9). For supershift reactions, 1 μl of anti-p50 or -p65 antibody (sc-114X or sc-472X; Santa Cruz, Paso Robles, CA) was added after 20 min of binding reaction, with further incubation for 30 min on ice. Samples were resolved on a 5% acrylamide gel in 0.25% Tris-borate-EDTA buffer.

Echocardiographic and hemodynamic measurements. Four weeks after the operation, mice underwent physiological evaluation with echocardiography and left heart catheterization as previously reported (20). After anesthetization with pentobarbital sodium (30 mg/kg body wt ip, Abbott), a mouse was positioned supine. A 7.5-MHz transducer connected to a dedicated ultrasonographic system (SSD-5500 ALOKA) was applied to the left hemithorax. Two-dimensional targeted M-mode imaging was obtained from the short-axis view at the level of the greatest left ventricular (LV) dimension. After echocardiography, a 1.4-F micromanometer-tipped catheter (Millar Instruments) was inserted into the right carotid artery and then advanced into the LV for pressure measurement under additional anesthesia with 2.5% Avertin (3 μl/g body wt ip, Aldrich Chemical).

Infarct size and myocardial histopathology. After hemodynamic study, the heart was excised and fixed in 4% paraformaldehyde for the evaluation of infarct size and histopathology. Infarct size was determined by methods described previously for rats (17) and also for mice (16, 20). Briefly, the LV was cut from apex to base into four transverse sections. Five-micrometer sections were sliced and stained with Masson's trichrome. Infarct length was measured along the endocardial and epicardial surfaces from each of the LV sections, and the values from all specimens were summed. Total LV circumference was calculated as the sum of endocardial and epicardial segment lengths from all LV sections. Infarct size (in percent) was calculated as total infarct circumference divided by total LV circumference. Cross-sectional area of cardiomyocytes and collagen volume fraction of noninfarct myocardium were determined by quantitative morphometry of tissue sections as previously reported (20).

RNase protection assay. Multiprobe RNase protection assay (RPA) was performed according to the manufacture's protocol (RiboQuant, PharMingen) with 5 μg of total RNA (8, 9). A custom template set containing murine TNF-α; IL-1β; IL-6; transforming growth factor (TGF)-β1; regulated on activation, normal T cell expressed and secreted (RANTES); monocyte chemoattractant protein (MCP)-1; and glyceraldehyde-3-phosphate dehydrogenase (GAPDH) was applied. After RNase digestion, protected probes were resolved on denaturing polyacrylamide gels and quantified by NIH image. The value of each hybridized probe was normalized to that of GAPDH included in each template set as an internal control.

Activity of MAPK. Western blotting analysis was performed by methods described previously (9). Briefly, the noninfarct LV was homogenized with a lysis buffer containing 25 mM Tris, pH 7.4, 150 mM NaCl, 5 mM EDTA, 1 mM Na_3VO_4, 10 mM NaF, 1% (vol/vol) Triton X-100, and 1% (vol/vol) glycerol. Equal amounts of the heart homogenate (30 μg) were separated by SDS-PAGE on 10% (wt/vol) gels, transferred onto a nitrocellulose membrane (Trans-Blot Transfer Medium, Bio-Rad Lab), and blocked with 5% skimmed milk at room temperature for 60 min. The membranes were subjected to immunoblot analyses with anti-phospho-extracellular signal-regulated kinase (ERK) antibody (no. 9106; Cell Signaling Technology), anti-phospho-c-Jun NH_2-terminal kinase (JNK) antibody (no. 9255; Cell Signaling Technology), or anti-phospho-p38 antibody (no. 9211; Cell Signaling Technology). Duplicate samples were subjected to immunoblot analyses with anti-ERK antibody (no. 9102; Cell Signaling Technology), anti-JNK1 antibody (sc-474; Santa Cruz Biotechnology), or anti-p38 antibody (no. 9212; Cell Signaling Technology). Immunodetection was accomplished with a horseradish anti-rabbit or anti-mouse secondary antibody (1:2,000 dilution, Amersham) by using an enhanced chemiluminescence kit (Amersham).

Evaluation of infarct size 24 h after coronary ligation. Evans blue dye (1%) was perfused into the aorta and coronary arteries, and tissue sections were weighed and then incubated with a 1.5% triphenyltetrazolium chloride solution at 37°C for 20 min. The infarct area (pale area), the area at risk (nonblue area), and the total LV area from each section were measured, multiplied by the weight of the section, and then totaled from all sections (20).

DNA ladder. Genomic DNA was isolated from the LV using a proteinase K method as previously described (20). To visualize the DNA laddering, fragmented DNA was amplified by ligation-mediated PCR (Maxim Biotech, South San Francisco, CA). Briefly, after overnight ligation with specially designed adapters, 25 ng of DNA in 50 μl of solution was amplified with 35 cycles of PCR and resolved on a 1.5% agarose/ethidium bromide gel.

Statistics. Results are presented as means ± SD. Survival analysis was performed by the Kaplan-Meier methods. ANOVA with Student-Newman-Keuls post hoc test or χ^2 test was used for statistical comparison. Differences were considered significant at a value of $P < 0.05$.

RESULTS

Activation of NF-κB in infarct and noninfarct myocardium. EMSA was performed with nuclear protein isolated from infarct myocardium 24 h after MI and noninfarct myocardium 7 days after MI. Compared with WT + sham-operated mice, NF-κB was further activated in infarct (Fig. 1*A*) and noninfarct myocardium (Fig. 1*B*) of WT + MI mice. In contrast, activation of NF-κB was completely abolished in KO + sham-operated and KO + MI mice. Most of NF-κB band in infarct myocardium was supershifted with the anti-p50 antibody (Fig. 1*C*), suggesting that the majority of NF-κB was p50-p50 homodimers or p50-p65 heterodimers.

Improved survival after MI in NF-κB KO mice. Within 24 h after the operation, 44 of 119 WT + MI (37%) and 46 of 121 KO + MI mice (38%, $P = 0.973$) died of cardiogenic shock without ventricular rupture or bleeding. In contrast, none of 16 WT + sham-operated and 20 KO + sham-operated mice died after the operation. Survival analysis was performed up to 12 wk in these survived animals. Within 7 days after MI, 25 of 75 WT + MI (33%) and 19 of 75 KO + MI mice (25%, $P = 0.370$) died. Although the total mortality was not different statistically, the rate of ventricular rupture was significantly lower in KO + MI mice (11 of 75) than WT + MI mice (22 of 75, $P < 0.05$). As shown in Fig. 2, the survival rate up to 12 wk after MI was significantly higher in KO + MI mice (73.3%) than WT + MI mice (56.0%, $P < 0.05$). No ventricular rupture was observed after 7 days. All the autopsied mice exhibited marked cardiomegaly and pleural effusion, suggest-

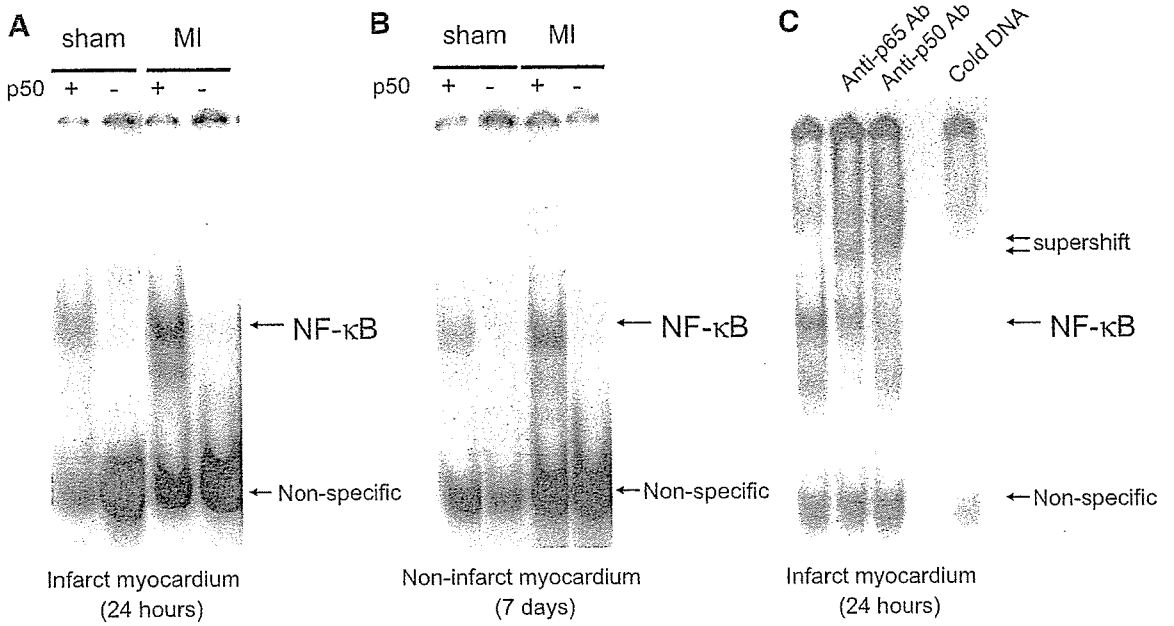

Fig. 1. Electrophoretic mobility shift assay for activated NF-κB after myocardial infarction (MI) in the presence (+) or absence (−) of the p50 subunit. Nuclear proteins were isolated from infarct myocardium 24 h after MI (*A*) and noninfarct myocardium 7 days after MI (*B*). Nuclear proteins were isolated from the corresponding myocardium in sham-operated mice. Supershift analysis was performed by using anti-p50 or -p65 antibody (Ab) to investigate the subunit composition of activated NF-κB in infarct myocardium (*C*).

ing that they died of congestive heart failure. These results suggest that blockade of NF-κB may prevent ventricular rupture early after MI and improve the survival with ameliorating congestive heart failure thereafter.

Attenuated cardiac dysfunction in KO + MI mice. Cardiac function was evaluated 4 wk after the operation by using echocardiography and left heart catheterization. The results are summarized in Table 1. Echocardiography revealed no significant differences in cardiac morphology and function between WT + sham-operated and KO + sham-operated mice. Although both WT + MI and KO + MI mice had significantly larger LV dimensions and significantly lower fractional shortening than WT + sham-operated mice, LV systolic dimension was significantly smaller and fractional shortening was significantly higher in KO + MI mice than in WT + MI mice.

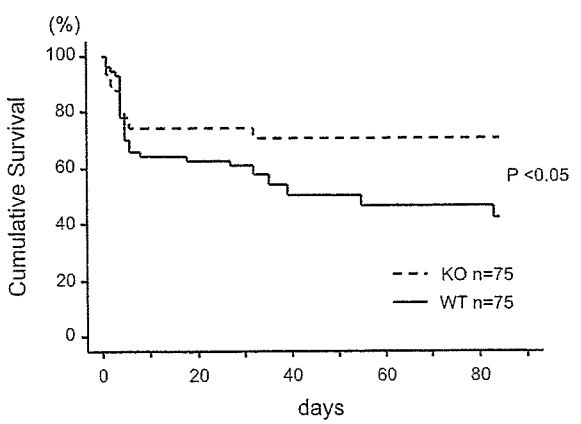

Fig. 2. Kaplan-Meier survival curves of wild-type (WT) and NF-κB knockout mice (KO) after MI.

As in echocardiographic parameters, LV pressure parameters were not significantly different between WT + sham-operated and KO + sham-operated mice. LV systolic pressure, maximum rate of rise of LV pressure ($+dP/dt_{max}$), and peak rate of LV pressure fall ($-dP/dt_{min}$) were significantly lower and LV end-diastolic pressure was significantly higher in WT + MI mice than in WT + sham-operated mice. In contrast, there were no significant differences in LV systolic pressure, $+dP/dt_{max}$, $-dP/dt_{min}$, and end-diastolic pressure between KO + sham-operated and KO + MI mice. LV systolic pressure and $+dP/dt_{max}$ were significantly higher and LV end-diastolic pressure was significantly lower in KO + MI mice than WT + MI mice. These results suggest that LV dysfunction after MI was significantly ameliorated in KO mice.

Infarct size was evaluated after hemodynamic evaluation in each mouse. Because infarct size was not different between WT + MI and KO + MI mice (Table 1), the differences in cardiac function were not attributable to infarct size variation.

Amelioration of myocyte hypertrophy and interstitial fibrosis in KO + MI mice. Table 2 summarizes the heart and lung weights 4 wk after the operation. Compared with WT + sham-operated mice, there were significant increases in LV weight, atrial weight, and lung weight in WT + MI mice, consistent with the increased LV end-diastolic pressure after MI. No differences in RV weight, LV weight, atrial weight, and lung weight were observed between WT + sham-operated and KO + sham-operated mice. Compared with WT + MI mice, there were significant decreases in atrial weight and lung weight in KO + MI mice, in agreement with the attenuated elevation of LV end-diastolic pressure in KO + MI mice.

Cross-sectional area of cardiomyocytes and collagen volume fraction of noninfarct myocardium were evaluated with Masson-trichrome staining (Fig. 3*A*). As summarized in Fig. 3*B*,

Table 1. *Left ventricular function and infarct size*

	WT + Sham Operated	KO + Sham Operated	WT + MI	KO + MI
n	6	6	12	13
Echocardiographic data				
Heart rate, beats/min	464±49	467±58	444±58	444±48
End-diastolic dimension, mm	3.38±0.31	3.20±0.30	5.09±0.50*	4.91±0.48*
End-systolic dimension, mm	1.80±0.36	1.62±0.19	4.30±0.57*	3.86±0.46*†
Fractional shortening, %	46.7±5.9	49.0±1.7	15.8±3.8*	21.7±3.7*†
Infarct wall thickness, mm	NA	NA	0.41±0.07	0.48±0.08
Noninfarct wall thickness, mm	0.97±0.16	0.97±0.10	1.14±0.18	1.08±0.08
Hemodynamic data				
Heart rate, beats/min	414±21	399±35	407±28	417±30
Systolic pressure, mmHg	94.8±5.3	95.7±7.0	86.0±9.0*	96.2±9.6†
End-diastolic pressure, mmHg	1.8±2.1	2.1±1.9	7.9±4.9*	4.5±4.6†
$+dP/dt_{max}$, mmHg/s	9,655±2,403	9,655±742	6,562±1,516*	8,231±1,844†
$-dP/dt_{min}$, mmHg/s	5,485±799	4,660±736	3,814±865*	4,378±875*
Infarct size, %	NA	NA	44.9±6.1	45.3±6.9

Data are means ± SD; *n* indicates no. of animals studied. NA, not applicable. KO, NF-κB knockout; $+dP/dt_{max}$, maximum rate of rise of left ventricular pressure; $-dP/dt_{min}$, peak rate of left ventricular pressure fall. *$P < 0.05$ vs. wild type (WT) + sham operated; †$P < 0.05$ vs. WT + myocardial infarction (MI).

the cross-sectional area of cardiomyocytes in noninfarct myocardium was significantly increased in WT + MI mice. In contrast, the cross-sectional area was not increased statistically in KO + MI mice. As summarized in Fig. 3*C*, collagen volume fraction was significantly increased in WT + MI mice compared with WT + sham-operated mice and was smaller in KO + MI mice. These results indicated that myocyte hypertrophy and interstitial fibrosis in noninfarct myocardium after MI were attenuated in KO mice.

Myocardial expression of cytokines. Expression of proinflammatory cytokines was assessed by multiprobe RPA (Fig. 4). Proinflammatory cytokines and chemokines, including RANTES, TNF-α, IL-1β, IL-6, TGF-β, and MCP-1, were upregulated in infarct myocardium 24 h after MI in KO mice as well as in WT mice (Fig. 4, *A* and *B*). Although we had expected that the expression of proinflammatory cytokines and chemokines would be attenuated by NF-κB KO, there were no differences in the expression of IL-1β, IL-6, TGF-β, and MCP-1 between WT + MI and KO + MI mice. On the contrary, the expression of RANTES and TNF-α was enhanced in KO + MI mice.

As in the infarct myocardium, expression of proinflammatory cytokines was evaluated in noninfarct myocardium 4 wk after MI (Fig. 4, *C* and *D*). Compared with WT + sham-operated mice, expression of TNF-α and IL-6 was significantly increased in the noninfarct myocardium of WT + MI mice. Blockade of NF-κB activation did not affect IL-6 but rather enhanced TNF-α expression in KO + MI mice. These results suggest that the induction of proinflammatory cytokines in infarct and noninfarct myocardium was mediated by NF-κB-independent pathways.

Phosphorylation of MAP kinases. Activation of MAP kinases has been shown to play an important role in cardiac hypertrophy and remodeling. As shown in Fig. 5, both ERK and JNK, but not p38, were phosphorylated in noninfarct myocardium 7 days after MI in WT mice. There were no significant differences in the protein levels of ERK, JNK, or p38 between WT and KO mice. However, NF-κB KO almost completely abolished the phosphorylation of JNK, although it did not affect that of ERK. The selective abrogation of JNK phosphorylation might play an important role in the attenuation of cardiac remodeling and dysfunction after MI in KO mice.

Infarct size and apoptosis 24 h after MI. Because the rate of ventricular rupture was significantly lower in KO + MI mice, another group of animals with WT + MI ($n = 5$) and KO + MI ($n = 6$) were evaluated at 24 h after MI to elucidate the underlying mechanisms. As summarized in Table 3, the infarct area in KO + MI mice was significantly lower than that in WT + MI mice, which may suggest less myocardial damage early after MI in KO mice. As indicated by the DNA ladder assay, although apoptosis was increased in the infarct myocardium at 24 h after MI, the extent of apoptosis was not different between WT and KO mice (Fig. 6). Therefore, the difference in infarct size may not be attributed to apoptosis.

Table 2. *Heart and lung weights*

	WT + Sham Operated	KO + Sham Operated	WT + MI	KO + MI
n	6	6	13	13
BW, g	30.7±1.5	30.6±2.5	29.9±1.7	30.0±1.9
Heart weight/BW, mg/g	4.31±0.71	4.28±0.49	5.71±0.75*	4.99±0.49*†
Left ventricular weight/BW, mg/g	2.89±0.49	2.80±0.28	3.64±0.64*	3.23±0.42
Right ventricular weight/BW, mg/g	0.75±0.18	0.85±0.20	0.76±0.25	0.78±0.12
Atrial weight/BW, mg/g	0.68±0.23	0.63±0.24	1.30±0.37*	0.97±0.28
Lung weight/BW, mg/g	4.91±0.55	5.02±0.77	6.62±1.37*	5.05±0.62†

Data are means ± SD; *n* indicates no. of animals studied; BW, body weight. *$P < 0.05$ vs. WT + sham operated; †$P < 0.05$ vs. WT + MI.

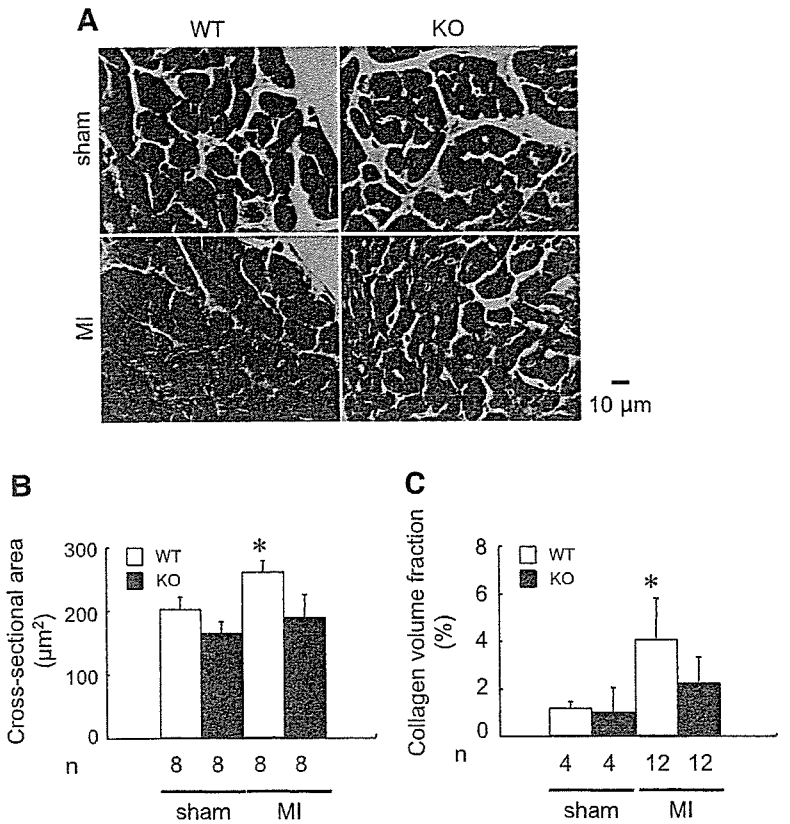

Fig. 3. Histology of noninfarct myocardium 4 wk after sham or left coronary artery ligation (MI). *A*: representative micrographs of Masson-trichrome staining for wild-type (WT) and NF-κB-KO mice. *B*: summarized data of cross-sectional area of cardiomyocytes. *C*: summarized data of collagen volume fraction. Values are means ± SD. $^*P < 0.05$ vs. WT + sham operated.

DISCUSSION

In the present study, we investigated the role of NF-κB in the pathogenesis of cardiac remodeling and heart failure after MI. We confirmed that NF-κB was activated in noninfarct as well as infarct myocardium in WT + MI mice. Targeted disruption of the p50 subunit of NF-κB abrogated the activation of NF-κB and ameliorated myocyte hypertrophy, interstitial fibrosis, and cardiac dysfunction in KO + MI mice, indicating that cardiac remodeling and heart failure after MI is mediated by the activation of NF-κB. In contrast, induction of proinflammatory cytokines and chemokines was not ameliorated but rather enhanced in KO + MI mice, suggesting that myocardial inflammation after MI might be mediated by NF-κB-independent pathways. Although the precise mechanisms by which blockade of NF-κB ameliorated cardiac dysfunction and heart failure after MI remain undetermined, selective abrogation of JNK phosphorylation in KO mice might play an important role. These results indicate that blockade of NF-κB might be a new therapeutic strategy to prevent ventricular remodeling and heart failure after MI.

The role of NF-κB activation in acute myocardial ischemia remains controversial and might be different between transient and sustained myocardial ischemia. Studies using a model of ischemia-reperfusion injury have shown that blockade of NF-κB reduces infarct size and protects myocytes from ischemic insult (2, 15). In contrast, a study using a model of permanent coronary ligation has reported that blockade of NF-κB promotes myocyte apoptosis and increases infarct size 24 h after MI (14). However, the long-term effects of NF-κB blockade after permanent coronary ligation have not been investigated. In the present study, we used a MI model of permanent coronary ligation to evaluate the long-term effects of NF-κB blockade on ventricular remodeling and heart failure. Because we ligated the coronary artery carefully to ensure that the area at risk was consistent, the infarct size evaluated 4 wk after MI was not different between WT + MI and KO + MI mice. However, the rate of ventricular rupture was significantly different between WT + MI and KO + MI mice. All the ventricular ruptures occurred within 7 days after MI, and the incidence was twice higher in WT + MI mice. Because ventricular rupture may reflect an imbalance between myocardial death and repair, the reduction of ventricular rupture in KO + MI mice suggests that blockade of NF-κB might have retarded myocardial cell death and/or enhanced tissue repair and scar formation to maintain integrity of the infarct myocardium. Taken together, these results suggest that the net effect of NF-κB blockade is not harmful but desirable even after permanent occlusion of coronary arteries.

We have previously reported that blockade of NF-κB ameliorates myocardial hypertrophy in response to chronic infusion of ANG II (9) and improves cardiac function and survival in TNF-α-induced cardiomyopathy (8). In the present study, we have demonstrated that blockade of NF-κB improves cardiac function and survival after MI with

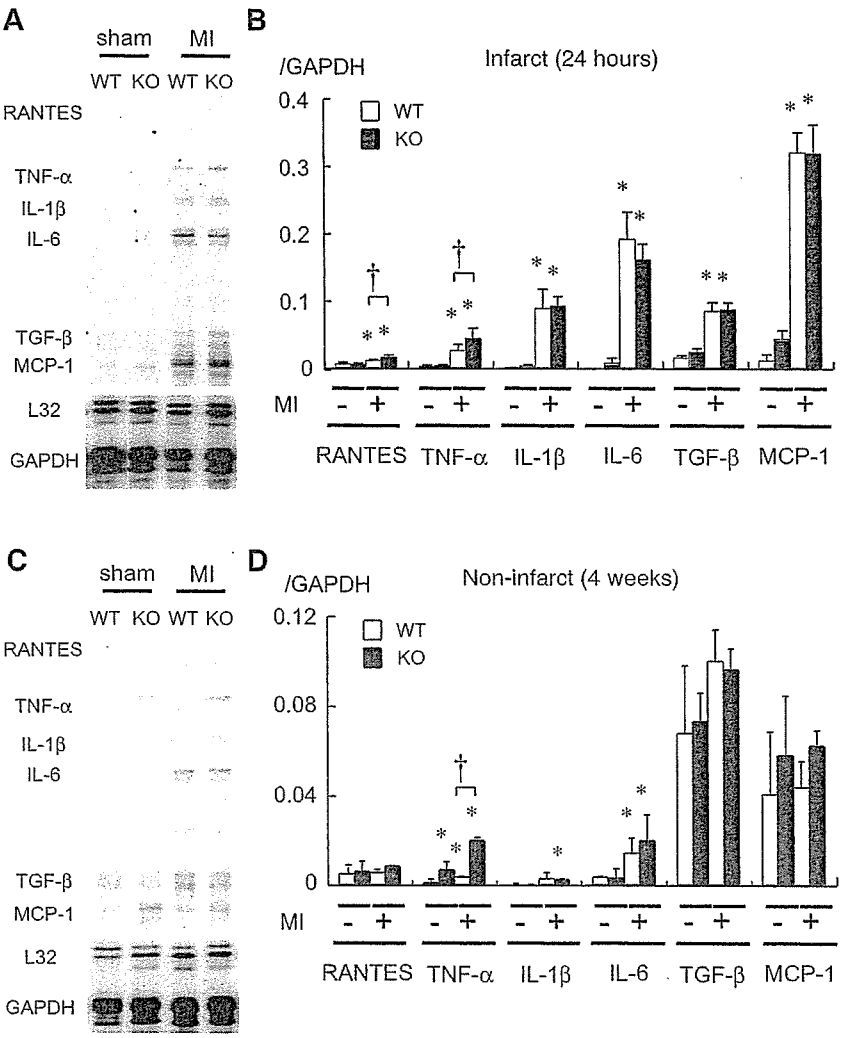

Fig. 4. Expression of proinflammatory cytokines and chemokines after MI. RNA was extracted from infarct myocardium 24 h after MI (*A*, *B*) and noninfarct myocardium 4 wk after MI (*C*, *D*) in WT and NF-κB-KO mice. Representative gels of multiprobe RNase protection assay (RPA) are shown in *A* and *C*, and summarized data are shown in *B* and *D*. The no. of animals are as follows: WT + sham operated (n = 3), KO + sham operated (n = 3), WT + MI (n = 5), KO + MI (n = 4) for infarct myocardium (*B*); WT + sham operated (n = 4), KO + sham operated (n = 5), WT + MI (n = 4), KO + MI (n = 3) for noninfarct myocardium (*D*). Values are means ± SD. TGF-β, transforming growth factor-β; RANTES, regulated on activation, normal T cell expressed and secreted; MCP-1, monocyte chemoattractant protein-1. *P < 0.05 vs. WT + sham operated, †P < 0.05 vs. WT + MI.

amelioration of myocyte hypertrophy and interstitial fibrosis. Although the precise mechanisms by which NF-κB promotes myocyte hypertrophy remain undetermined, it is of interest that phosphorylation of JNK was abrogated in p50-knockout mice. Because the protein level of JNK is not affected in p50-knockout mice, expression or activation of upstream kinases may be modulated by NF-κB pathways. MAP kinase signaling pathways, including ERK, JNK, and p38, are supposed to play an important role in cardiac hypertrophy and remodeling because they are phosphorylated and activated by G protein-coupled receptor agonists such as phenylephrine, endothelin-1, and ANG II (3, 21). Especially, JNK is also termed the stress-activated protein kinase because it is additionally activated by cellular stresses such as reactive oxygen species and proinflammatory cytokines, including IL-1β and TNF-α (21). Substrates of JNK are transcription factors, including c-Jun, ATF2, and Elk1 (21). Inhibition of JNK has been shown to abrogate ventricular hypertrophy in vivo in response to pressure overload (4) or $G_{\alpha}q$ overexpression (13). Therefore, the attenuated myocyte hypertrophy after MI in p50-knockout mice may be mediated by the abrogation of the JNK pathways.

Although activation of NF-κB has been shown to induce various proinflammatory cytokines and chemokines, including TNF-α (1), we have previously reported that expression of proinflammatory cytokines in response to chronic infusion of ANG II or TNF-α-induced cardiomyopathy was not abrogated by targeted disruption of the p50 subunit of NF-κB (8, 9). In the present study, expression of proinflammatory cytokines in infarct and noninfarct myocardium was not ameliorated but rather enhanced in KO + MI mice. These results suggest that expression of proinflammatory cytokines in the failing heart may be mediated by NF-κB-independent pathways. Because blockade of NF-κB improved cardiac function with amelioration of myocyte hypertrophy and interstitial fibrosis in KO + MI mice, myocardial expression of proinflammatory cytokines may not be harmful in the progression of ventricular remodeling and heart failure after MI unless NF-κB is activated.

The paradoxical increase of TNF-α and RANTES in KO + MI mice might be explained by the difference in tran-

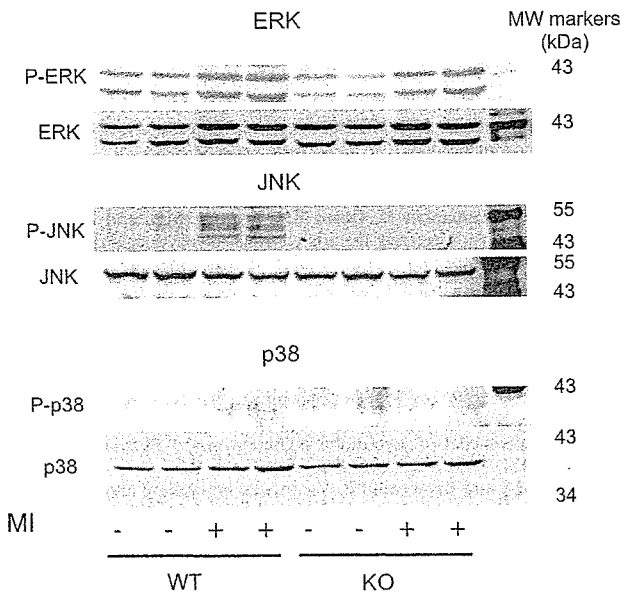

Fig. 5. Western blot analysis of ERK, JNK, and p38 with anti-phosphospecific (P-ERK, P-JNK, P-p38) or nonphosphospecific (ERK, JNK, p38) antibodies 7 days after MI. KO, NF-κB knockout mice.

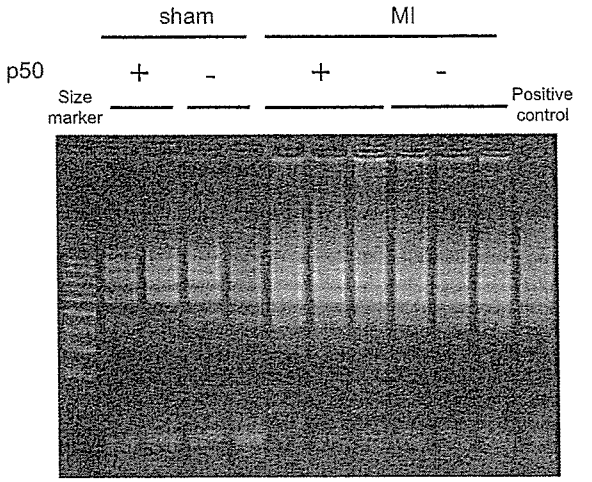

Fig. 6. Ligation-mediated PCR assay to demonstrate DNA laddering of samples prepared from sham-operated mice and infarct myocardium 24 h after MI.

scriptional activity of the p50-p65 heterodimer and p50-p50 homodimer (11). The NF-κB/Rel family consists of five subunit members: p50, p52, c-Rel, RelA (p65), and RelB. In most cells, NF-κB is a heterodimer of p50 and p65 that exists in the cytoplasm and is bound to the inhibitory protein IκB. Activation of NF-κB occurs when specific IκB kinases phosphorylate the IκB. After chronic exposure to proinflammatory cytokines, including TNF-α, NF-κB is converted from the transcriptionally active p50-p65 heterodimer to the transcriptionally inactive p50-p50 homodimer (6, 11), which may act as a native negative-feedback mechanism to prevent excessive inflammatory responses. The absence of p50-p50 homodimers in mice with targeted disruption of the p50 subunit therefore may account for enhanced expression of TNF-α and RANTES in KO + MI mice.

The cross-sectional area of cardiomyocytes in noninfarct myocardium was significantly increased in WT + MI mice. However, the wall thickness evaluated by echocardiography was not statistically different between WT + sham-operated and WT + MI mice. This might be explained as follows. Although the difference was not statistically significant, there was a trend of increased wall thickness in MI mice. The WT + MI to WT + sham-operated ratio of noninfarct wall thickness was 1.14/0.97 = 1.18. On the other hand, the cross-sectional area of myocyte in WT + MI mice was significantly greater than that in WT + sham-operated mice, with a ratio of 260/201 = 1.29. Because area is a two-dimensional parameter, the square root of cross-sectional area should correlate with wall thickness. Indeed, the square root of 1.29 is 1.14, which is close to the ratio of wall thickness of 1.18. Because the resolution of echocardiography is limited, it might not be able to consistently differentiate differences in thickness of <20%.

Table 3. *Area at risk and infarct area 24 h after coronary ligation*

	WT + MI	KO + MI
n	5	6
Area at risk, %	39.7±2.98	37.9±2.68
Infarct area, %	20.6±2.80	14.9±2.21*
Infarct area/area at risk, %	52.1±5.90	39.4±6.96*

Data are means ± SD; *n* indicates no. of animals studied. *$P < 0.05$ vs. WT + MI.

In the present study, to achieve complete and chronic inhibition of NF-κB in vivo, we used gene-manipulated mice lacking the p50 subunit of NF-κB. These mice show no developmental abnormalities but exhibit multifocal defects in B-cell-mediated immune responses and nonspecific responses to infection. In these animals, B cells do not proliferate in response to bacterial lipopolysaccharide and are defective in basal and specific antibody production (19). Although we did not detect any adverse effects or premature death in the p50-knockout mice during the observation period, systemic inhibition of NF-κB may be deleterious in the long run. Therefore, it may be desirable to employ cardiac-specific inhibition of NF-κB to minimize immunological detrimental effects. Furthermore, the results observed in gene-manipulated mice may be different from the outcomes of pharmacological interventions because an inherent deficit of a specific gene may alter the expression and functions of other genes as compensation mechanisms. Therefore, further studies are required to draw a final conclusion that blockade of NF-κB is beneficial and applicable as a therapeutic strategy for patients with MI.

GRANTS

A part of this study was conducted in Kyushu University Station for Collaborative Research. This study was supported by a grant from Kimura Memorial Heart Foundation, by the Grant for Research on Cardiovascular Disease from Japan Heart Foundation/Pfizer Pharmaceuticals, and by the Grant-in-Aid for Scientific Research from the Japan Society for the Promotion of Science (C15590755).

REFERENCES

1. **Barnes PJ and Karin M.** Nuclear factor-κB: a pivotal transcription factor in chronic inflammatory diseases. *N Engl J Med* 336: 1066–1071, 1997.
2. **Brown M, McGuinness M, Wright T, Ren X, Wang Y, Boivin GP, Hahn H, Feldman AM, and Jones WK.** Cardiac-specific blockade of NF-κB in cardiac pathophysiology: differences between acute and chronic stimuli in vivo. *Am J Physiol Heart Circ Physiol* 289: H466–H476, 2005.
3. **Bueno OF and Molkentin JD.** Involvement of extracellular signal-regulated kinases 1/2 in cardiac hypertrophy and cell death. *Circ Res* 91: 776–781, 2002.
4. **Choukroun G, Hajjar R, Fry S, del Monte F, Haq S, Guerrero JL, Picard M, Rosenzweig A, and Force T.** Regulation of cardiac hypertrophy in vivo by the stress-activated protein kinases/c-Jun NH_2-terminal kinases. *J Clin Invest* 104: 391–398, 1999.
5. **Grabellus F, Levkau B, Sokoll A, Welp H, Schmid C, Deng MC, Takeda A, Breithardt G, and Baba HA.** Reversible activation of nuclear factor-κB in human end-stage heart failure after left ventricular mechanical support. *Cardiovasc Res* 53: 124–130, 2002.
6. **Haudek SB, Bryant DD, and Giroir BP.** Differential regulation of myocardial NFκB following acute or chronic TNF-α exposure. *J Mol Cell Cardiol* 33: 1263–1271, 2001.
7. **Hirotani S, Otsu K, Nishida K, Higuchi Y, Morita T, Nakayama H, Yamaguchi O, Mano T, Matsumura Y, Ueno H, Tada M, and Hori M.** Involvement of nuclear factor-κB and apoptosis signal-regulating kinase 1 in G-protein-coupled receptor agonist-induced cardiomyocyte hypertrophy. *Circulation* 105: 509–515, 2002.
8. **Kawamura N, Kubota T, Kawano S, Monden Y, Feldman AM, Tsutsui H, Takeshita A, and Sunagawa K.** Blockade of NF-κB improves cardiac function and survival without affecting inflammation in TNF-α-induced cardiomyopathy. *Cardiovasc Res* 66: 520–529, 2005.
9. **Kawano S, Kubota T, Monden Y, Kawamura N, Tsutsui H, Takeshita A, and Sunagawa K.** Blockade of NF-κB ameliorates myocardial hypertrophy in response to chronic infusion of angiotensin II. *Cardiovasc Res* 67: 689–698, 2005.
10. **Kubota T, Miyagishima M, Alvarez RJ, Kormos R, Rosenblum WD, Demetris AJ, Semigran MJ, Dec GW, Holubkov R, McTiernan CF, Mann DL, Feldman AM, and McNamara DM.** Expression of proinflammatory cytokines in the failing human heart: comparison of recent-onset and end-stage congestive heart failure. *J Heart Lung Transplant* 19: 819–824, 2000.
11. **Lawrence T, Gilroy DW, Colville-Nash PR, and Willoughby DA.** Possible new role for NF-κB in the resolution of inflammation. *Nat Med* 7: 1291–1297, 2001.
12. **Li Y, Ha T, Gao X, Kelley J, Williams DL, Browder IW, Kao RL, and Li C.** NF-κB activation is required for the development of cardiac hypertrophy in vivo. *Am J Physiol Heart Circ Physiol* 287: H1712–H1720, 2004.
13. **Minamino T, Yujiri T, Terada N, Taffet GE, Michael LH, Johnson GL, and Schneider MD.** MEKK1 is essential for cardiac hypertrophy and dysfunction induced by Gq. *Proc Natl Acad Sci USA* 99: 3866–3871, 2002.
14. **Misra A, Haudek SB, Knuefermann P, Vallejo JG, Chen ZJ, Michael LH, Sivasubramanian N, Olson EN, Entman ML, and Mann DL.** Nuclear factor-κB protects the adult cardiac myocyte against ischemia-induced apoptosis in a murine model of acute myocardial infarction. *Circulation* 108: 3075–3078, 2003.
15. **Morishita R, Sugimoto T, Aoki M, Kida I, Tomita N, Moriguchi A, Maeda K, Sawa Y, Kaneda Y, Higaki J, and Ogihara T.** In vivo transfection of cis element "decoy" against nuclear factor-κB binding site prevents myocardial infarction. *Nat Med* 3: 894–899, 1997.
16. **Patten RD, Aronovitz MJ, Deras-Mejia L, Pandian NG, Hanak GG, Smith JJ, Mendelsohn ME, and Konstam MA.** Ventricular remodeling in a mouse model of myocardial infarction. *Am J Physiol Heart Circ Physiol* 274: H1812–H1820, 1998.
17. **Pfeffer MA and Braunwald E.** Ventricular remodeling after myocardial infarction. Experimental observations and clinical implications. *Circulation* 81: 1161–1172, 1990.
18. **Purcell NH, Tang G, Yu C, Mercurio F, DiDonato JA, and Lin A.** Activation of NF-κB is required for hypertrophic growth of primary rat neonatal ventricular cardiomyocytes. *Proc Natl Acad Sci USA* 98: 6668–6673, 2001.
19. **Sha WC, Liou HC, Tuomanen EI, and Baltimore D.** Targeted disruption of the p50 subunit of NF-κB leads to multifocal defects in immune responses. *Cell* 80: 321–330, 1995.
20. **Shiomi T, Tsutsui H, Matsusaka H, Murakami K, Hayashidani S, Ikeuchi M, Wen J, Kubota T, Utsumi H, and Takeshita A.** Overexpression of glutathione peroxidase prevents left ventricular remodeling and failure after myocardial infarction in mice. *Circulation* 109: 544–549, 2004.
21. **Sugden PH and Clerk A.** "Stress-responsive" mitogen-activated protein kinases (c-Jun N-terminal kinases and p38 mitogen-activated protein kinases) in the myocardium. *Circ Res* 83: 345–352, 1998.
22. **Torre-Amione G, Kapadia S, Lee J, Durand JB, Bies RD, Young JB, and Mann DL.** Tumor necrosis factor-α and tumor necrosis factor receptors in the failing human heart. *Circulation* 93: 704–711, 1996.
23. **Wong SC, Fukuchi M, Melnyk P, Rodger I, and Giaid A.** Induction of cyclooxygenase-2 and activation of nuclear factor-κB in myocardium of patients with congestive heart failure. *Circulation* 98: 100–103, 1998.

Circulation
JOURNAL OF THE AMERICAN HEART ASSOCIATION

American Heart Association®
Learn and Live℠

Overexpression of Mitochondrial Peroxiredoxin-3 Prevents Left Ventricular Remodeling and Failure After Myocardial Infarction in Mice

Shouji Matsushima, Tomomi Ide, Mayumi Yamato, Hidenori Matsusaka, Fumiyuki Hattori, Masaki Ikeuchi, Toru Kubota, Kenji Sunagawa, Yasuhiro Hasegawa, Tatsuya Kurihara, Shinzo Oikawa, Shintaro Kinugawa and Hiroyuki Tsutsui

Circulation 2006;113;1779-1786; originally published online Apr 3, 2006;
DOI: 10.1161/CIRCULATIONAHA.105.582239
Circulation is published by the American Heart Association. 7272 Greenville Avenue, Dallas, TX 72514
 Print ISSN: 0009-7322. Online ISSN: 1524-4539

Overexpression of Mitochondrial Peroxiredoxin-3 Prevents Left Ventricular Remodeling and Failure After Myocardial Infarction in Mice

Shouji Matsushima, MD; Tomomi Ide, MD, PhD; Mayumi Yamato, PhD; Hidenori Matsusaka, MD; Fumiyuki Hattori, PhD; Masaki Ikeuchi, MD; Toru Kubota, MD, PhD; Kenji Sunagawa, MD, PhD; Yasuhiro Hasegawa, PhD; Tatsuya Kurihara, PhD; Shinzo Oikawa, PhD; Shintaro Kinugawa, MD, PhD; Hiroyuki Tsutsui, MD, PhD

Background—Mitochondrial oxidative stress and damage play major roles in the development and progression of left ventricular (LV) remodeling and failure after myocardial infarction (MI). We hypothesized that overexpression of the mitochondrial antioxidant, peroxiredoxin-3 (Prx-3), could attenuate this deleterious process.

Methods and Results—We created MI in 12- to 16-week-old, male Prx-3–transgenic mice (TG+MI, n=37) and nontransgenic wild-type mice (WT+MI, n=39) by ligating the left coronary artery. Prx-3 protein levels were 1.8 times higher in the hearts from TG than WT mice, with no significant changes in other antioxidant enzymes. At 4 weeks after MI, LV thiobarbituric acid–reactive substances in the mitochondria were significantly lower in TG+MI than in WT+MI mice (mean±SEM, 1.5±0.2 vs 2.2±0.2 nmol/mg protein; n=8 each, $P<0.05$). LV cavity dilatation and dysfunction were attenuated in TG+MI compared with WT+MI mice, with no significant differences in infarct size (56±1% vs 55±1%; n=6 each, P=NS) and aortic pressure between groups. Mean LV end-diastolic pressures and lung weights in TG+MI mice were also larger than those in WT+sham-operated mice but smaller than those in WT+MI mice. Improvement in LV function in TG+MI mice was accompanied by a decrease in myocyte hypertrophy, interstitial fibrosis, and apoptosis in the noninfarcted LV. Mitochondrial DNA copy number and complex enzyme activities were significantly decreased in WT+MI mice, and this decrease was also ameliorated in TG+MI mice.

Conclusions—Overexpression of Prx-3 inhibited LV remodeling and failure after MI. Therapies designed to interfere with mitochondrial oxidative stress including the antioxidant Prx-3 might be beneficial in preventing cardiac failure. (***Circulation.* 2006;113:1779-1786.**)

Key Words: antioxidants ■ free radicals ■ heart failure ■ myocardial infarction ■ remodeling

Experimental and clinical studies have demonstrated excessive generation of reactive oxygen species (ROS) in failing hearts.[1,2] Among the potential sources of ROS within the heart, mitochondrial electron transport produces superoxide anion ($\cdot O_2^-$) in this disease state.[3] Furthermore, increased ROS leads to mitochondrial DNA (mtDNA) damage and dysfunction.[4,5] Therefore, the intimate link between mitochondrial oxidative stress, mtDNA decline, and mitochondrial dysfunction plays an important role in the development and progression of left ventricular (LV) remodeling and failure that occur after myocardial infarction (MI).

Clinical Perspective p 1786

Peroxiredoxin-3 (Prx-3) is a mitochondrial antioxidant protein and member of the Prx family that can scavenge H_2O_2 in cooperation with thiol and peroxynitrite.[6] In mammals, 6 distinct Prx family members have been identified (Prx-1 through -6). Among the Prxs, Prx-3 is unique because it is localized specifically within the mitochondria.[7] Furthermore, in vivo transfer of the *Prx-3* gene protected neurons against cell death induced by oxidative stress.[8] These beneficial characteristics make Prx-3 an important candidate for therapy against LV failure after MI, in which ROS production has been demonstrated to be increased within the mitochondria.[1,4] Although several previous reports showed the beneficial effects of antioxidants on heart failure,[9,10] no study has ever been performed to specifically examine the protective role of Prx-3. To address these questions, we created transgenic (TG) mice containing the rat *Prx-3* gene. Rat Prx-3–TG mice and their wild-type (WT) littermates were randomized to receive

Received August 10, 2005; revision received January 26, 2006; accepted February 2, 2006.

From the Department of Cardiovascular Medicine, Graduate School of Medical Sciences (S.M., T.I., H.M., M.I., T.K., K.S.), and the Department of Redox Medicinal Science, Graduate School of Pharmaceutical Sciences (M.Y.), Kyushu University, Fukuoka; Biomedical Research Laboratories (F.H., Y.H., T.K., S.O.), Daiichi Suntory Pharma Co, Ltd, Osaka; and the Department of Cardiovascular Medicine (S.K., H.T.), Hokkaido University Graduate School of Medicine, Sapporo, Japan.

Correspondence to Hiroyuki Tsutsui, MD, PhD, Department of Cardiovascular Medicine, Hokkaido University Graduate School of Medicine, Kita-15, Nishi-7, Kita-ku, Sapporo 060-8638, Japan. E-mail htsutsui@med.hokudai.ac.jp

Circulation is available at http://www.circulationaha.org

DOI: 10.1161/CIRCULATIONAHA.105.582239

either a large transmural MI induced by coronary artery ligation or sham operation.

Methods

Generation of TG Mice

The rat Prx-3 cDNA fragment including the entire open reading frame from nucleotide 5 to 802 was amplified by polymerase chain reaction (PCR) and cloned into pCRII (Invitrogen, Carlsbad, Calif). An expression vector for Prx-3 was constructed with pQBI25 (TaKaRa), and the gene for green fluorescent protein was removed at the site of *NheI-Bam*HI. A cytomegalovirus promoter–driven expression cassette containing rat Prx-3 cDNA in the sense orientation was purified by ultracentrifugation with CsCl. The pronuclei of fertilized eggs from hyperovulated C57BL/6J mice were randomly microinjected with this DNA construct. Tail clips and a PCR protocol to confirm the genotype were performed by one group of investigators. Homozygous TG mice and C57BL/6J WT mice were used at 12 to 16 weeks of age. The study was approved by our institutional animal research committee and conformed to the animal care guidelines of the American Physiological Society.

Creation of MI

We created MI in 12- to 16-week-old, male TG mice (TG+MI) and nontransgenic WT littermates (WT+MI) by ligating the left coronary artery. Sham operation without coronary artery ligation was also performed in WT (WT+sham) and TG (TG+sham) mice. This assignment procedure was performed with the use of numeric codes to identify the animals.

Prx-3 Protein

Prx-3 protein levels were analyzed in cardiac tissue homogenates by Western blot analysis with a monoclonal antibody against rat Prx-3. Our preliminary studies revealed that this antibody against rat Prx-3 cross-reacted with mouse Prx-3 as a single band of 25 kDa. In brief, the LV tissues were homogenized with lysis buffer (20 mmol/L Tris-HCl, 1 mmol/L EDTA, 1 mmol/L EGTA, and 1 mmol/L phenylmethylsulfonylfluoride; pH 7.4). After centrifugation, equal amounts of protein (5 μg protein/lane), estimated by the Bradford method with a protein assay (Bio-Rad, Hercules, Calif), were electrophoresed on a 15% sodium dodecyl sulfate–polyacrylamide gel and then electrophoretically transferred to a nitrocellulose membrane (Millipore, Billerica, Mass). After being blocked with 5% nonfat milk in phosphate-buffered saline (PBS) containing 0.05% Tween 20 at 4°C for 1 hour, the membrane was incubated with the first antibody and then with the peroxidase-linked second antibody (Amersham Pharmacia, Uppsala, Sweden). Chemiluminescence was detected with an enhanced chemiluminescence Western blot detection kit (Amersham Pharmacia) according to the manufacturer's recommendation.

To further assess the subcellular localization of Prx-3 protein, mitochondrial and cytoplasmic fractions were prepared from LVs and subjected to Western blot analysis. In brief, the LV tissues were homogenized at 4°C for 1 minute in 6 volumes of buffer consisting of 10 mmol/L HEPES-NaOH (pH 7.4), 1 mmol/L disodium EDTA, and 250 mmol/L sucrose. The homogenate was centrifuged at 4°C and 3000*g* for 10 minutes to remove any nuclear and myofibrillar debris, and the resultant supernatant was centrifuged at 10 000*g* for 10 minutes to separate any cardiac subcellular fractions. The supernatant was used for the cytoplasmic fraction assay. To isolate the mitochondrial fraction, the pellet was resuspended at 4°C in a buffer consisting of 10 mmol/L HEPES-NaOH (pH 7.4), 1 mmol/L sodium EDTA, and 250 mmol/L sucrose and was washed 3 times with the same buffer. Murine antibodies directed toward glyceraldehyde 3-phosphate dehydrogenase (GAPDH) and cytochrome oxidase (COX) subunit I were also used to verify the integrity of these subcellular fractions.

Immunohistochemistry

Frozen sections of cardiac tissues were incubated in the presence of 100 nmol/L MitoTracker Red CMXRos (Molecular Probes, Eugene, Ore) at 37°C for 20 minutes. We did not repeat the freeze/thaw procedure to avoid the loss of mitochondrial integrity. After being washed with PBS (10 mmol/L sodium phosphate, pH 7.4, and 150 mmol/L NaCl), the sections were fixed with 3.7% formaldehyde for 5 minutes. After being washed, the fixed sections were incubated with 100-fold–diluted anti-rat Prx-3 antibody (10 μg/mL) in PBS at 4°C overnight. Fluorescence images were taken with a confocal laser scanning microscope (Bio-Rad MRC 1024) with laser beams of 488 and 568 nm for excitation.

Myocardial Antioxidant Enzyme Activities and Lipid Peroxidation

For the subsequent biochemical studies, the myocardial tissues with MI were carefully dissected into 3 parts: one consisting of the infarcted LV, one consisting of the border zone LV with the peri-infarct rim (a 1-mm rim of normal-appearing tissue), and one consisting of the remaining noninfarcted (remote) LV. The antioxidant enzymatic activities of superoxide dismutase (SOD), catalase, and glutathione peroxidase (GSHPx) were measured in the noninfarcted LV.[11] The formation of lipid peroxides was measured in the mitochondrial fraction isolated from the LV myocardium with use of a biochemical assay with thiobarbituric acid–reactive substances (TBARS).[4]

Survival

A survival analysis was performed in WT+sham (n=15), TG+sham (n=14), WT+MI (n=39), and TG+MI (n=37) mice. During the study period of 4 weeks, the cages were inspected daily for deceased animals. All deceased mice were examined for the presence of MI as well as pleural effusion and cardiac rupture.

Echocardiographic and Hemodynamic Measurements

At 4 weeks after surgery, echocardiographic studies were performed under light anesthesia with tribromoethanol/amylene hydrate (2.5% wt/vol, 8 μL/g IP) and spontaneous respiration. Two-dimensional, targeted M-mode tracings were recorded at a paper speed of 50 mm/s. Under the same anesthesia with Avertin, a 1.4F micromanometer-tipped catheter (Millar Instruments, Houston, Tex) was inserted into the right carotid artery and then advanced into the LV to measure LV pressures. One subset of investigators who were not informed of the experimental group assignments performed the in vivo LV function studies.

Infarct Size

To measure infarct size 28 days after MI, the heart was excised and the LVs were cut from apex to base into 3 transverse sections. Five-micron sections were cut and stained with Masson's trichrome. Infarct length was measured along the endocardial and epicardial surfaces in each of the cardiac sections, and the values from all specimens were summed. Infarct size (as a percentage) was calculated as total infarct circumference divided by total cardiac circumference.[12]

In addition, to measure infarct size after 24 hours (when most animals were still alive), a separate group of animals including WT+MI (n=5) and TG+MI (n=5) mice was created by ligating the left coronary artery according to the same methods described earlier. After 24 hours of coronary artery ligation, Evans blue dye (1%) was perfused into the aorta and coronary arteries, and tissue sections were weighed and then incubated with a 1.5% triphenyltetrazolium chloride solution. The infarct area (pale), the area at risk (not blue), and the total LV area from each section were measured.[13] In our preliminary study, we confirmed excellent reliability of infarct size measurements, in which a morphometric method similar to that performed in this study was used. The intraobserver and interob-

server variabilities between 2 measurements divided by these means, expressed as a percentage, were each <5%.

Myocardial Histopathology and Apoptosis

Myocyte cross-sectional area and collagen volume fraction were determined by quantitative morphometry of tissue sections from the mid-LV. To detect apoptosis, tissue sections from the mid-LV were stained with terminal deoxynucleotidyl transferase–mediated dUTP nick end-labeling (TUNEL) staining. The number of TUNEL-positive cardiac myocyte nuclei was counted, and the data were normalized per 10^5 total nuclei identified by hematoxylin-positive staining in the same sections. The proportion of apoptotic cells was counted in the noninfarcted LV. We further examined whether apoptosis was present by the more sensitive ligation-mediated PCR fragmentation assays (Maxim Biotech, Inc, Rockville, Md).

mtDNA Copy Number

DNA was extracted from cardiac tissues, and a Southern blot analysis was performed to measure the mtDNA copy number, as described earlier.[4] Primers for the mtDNA probe corresponded to nucleotides 2424 to 3605 of the mouse mitochondrial genome, and those for the nuclear-encoded mouse 18S rRNA probe corresponded to nucleotides 435 to 1951 of the human 18S rRNA genome. The mtDNA levels were normalized to the abundance of the 18S rRNA gene run on the same gel.

Mitochondrial Complex Enzyme Activity

The specific activity of mitochondrial electron transport chain complex I (rotenone-sensitive NADH-ubiquinone oxidoreductase), complex II (succinate-ubiquinone oxidoreductase), complex III (ubiquinol–cytochrome *c* oxidoreductase), and complex IV (cytochrome *c* oxidase) was measured in myocardial tissues according to methods described previously.[4] All enzymatic activities were expressed as nanomoles per minute per milligram protein.

Plasma TBARS

The formation of TBARS in peripheral blood samples from WT+MI and TG+MI mice was measured by a fluorometric assay, as described previously.[14] In brief, 100 μL of whole blood was mixed with 1 mL of saline and centrifuged at 3000*g* for 15 minutes. The supernatant was mixed with $1/12$N H_2SO_4 and 10% phosphotungstic acid, and the mixture was centrifuged. The sediment was suspended in distilled water, 0.3% thiobarbituric acid, and 0.1% butylated hydroxytoluene. The reaction mixture was then heated at 100°C for 60 minutes in an oil bath. After being cooled with tap water, the mixture was extracted with *n*-butanol and centrifuged at 1600*g* for 15 minutes. The fluorescence intensity of the organic phase was measured by spectrofluorometry with a wavelength of 510-nm excitation and 550-nm emission. Malondialdehyde standards (Sigma-Aldrich, St. Louis, Mo) were included with each assay batch, and plasma TBARS were expressed as micromoles per gram of plasma protein in reference to these standards.

Statistical Analysis

Data are expressed as mean±SEM. Survival analysis was performed by the Kaplan-Meier method, and between-group differences in survival were tested by the log-rank test. A between-group comparison of means was performed by 1-way ANOVA, followed by *t* tests. The Bonferroni correction was applied for multiple comparisons of means. $P<0.05$ was considered statistically significant.

The authors had full access to the data and take full responsibility for their integrity. All authors have read and agreed to the manuscript as written.

Results

We investigated 4 groups of mice, WT+sham (n=15), TG+sham (n=14), WT+MI (n=39), and TG+MI (n=37), in the present study. A survival analysis was performed for all of these mice. Subsequent echocardiographic and hemodynamic measurements were performed in the 4-week survivors: 15 WT+sham, 14 TG+sham, 25 WT+MI, and 31 TG+MI mice. These measurements could not be accomplished in 4 WT+MI and 5 TG+MI mice owing to technical difficulties. Survivor mice were further divided into 2 groups: those studied for subsequent histological analysis, including infarct size, myocyte size, and collagen volume fraction measurements as well as TUNEL staining (5 WT+sham, 5 TG+sham, 8 WT+MI, and 8 TG+MI), and those for the biochemical assay, including antioxidant enzyme activity, Prx-3 protein levels, mitochondrial lipid peroxidation, mtDNA copy number, and mitochondrial complex enzyme activities (8 WT+sham, 8 TG+sham, 8 WT+MI, and 8 TG+MI). Infarct size was not measured in the mice that died.

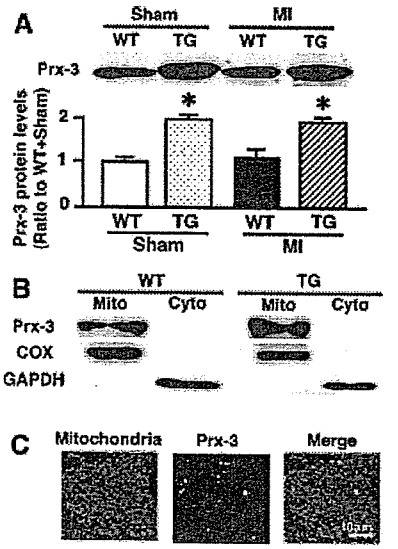

Figure 1. A, Representative Western blot analysis of Prx-3 protein levels (upper panels) and summary data (lower panels) in hearts from WT+sham, TG+sham, WT+MI, and TG+MI mice (n=6 each). Total protein extracts from the hearts were probed with a monoclonal antibody against rat Prx-3. The antibody recognized both rat and mouse Prx-3 as a single band of 25k Da. Data were obtained by densitometric quantification of the Western blots. Values are expressed as the ratio to the WT+sham value and mean±SEM. *$P<0.05$ for the difference from the ratio to WT+sham values. B, Localization of Prx-3 to mitochondria (mito). Western blot analysis of mitochondrial and cytoplasmic (cyto) fractions that were probed with antibodies directed toward Prx-3 as well as specific mitochondrial and cytoplasmic markers: GAPDH was detected in the cytoplasmic but not the mitochondrial fraction, and COX subunit I was detected in the mitochondrial but not the cytoplasmic fraction. Importantly, Prx-3 proteins were detected only in the mitochondrial fraction but not in the cytoplasmic fraction. C, Myocardial tissue sections from TG mice were doubly stained with MitoTracker dye (red) and a rat Prx-3–specific antibody (green). Immunoreactivity for Prx-3 was observed in the cytoplasm of cardiac myocytes. The merged images show that Prx-3 colocalized with the mitochondria (yellow). Scale bar=10 μm.

Myocardial Antioxidants and TBARS

First, baseline differences in Prx-3 proteins as well as other antioxidant enzyme activities between WT and TG mice were determined. In TG+sham, there was a significant increase in Prx-3 protein levels in the LV compared with that of WT+sham (Figure 1A). Importantly, the antioxidants, in-

TABLE 1. Characteristics of Animal Models

	WT+Sham	TG+Sham	WT+MI	TG+MI
Antioxidant enzymes				
n	7	7	7	7
SOD, U/mg protein	26.4±1.1	27.8±1.4	25.1±1.7	23.9±1.2
GSHPx, nmol/min per mg protein	74.1±3.2	77.7±6.7	87.8±4.8	86.1±4.2
Catalase, nmol/mg protein	79.9±6.4	85.0±6.2	87.1±3.5	81.4±5.8
Echocardiographic data				
n	15	14	21	26
Heart rate, bpm	481±11	451±8	463±13	458±8
LVEDD, mm	3.47±0.05	3.37±0.08	5.51±0.13†	4.9±0.10†§
LVESD, mm	2.22±0.05	2.12±0.10	4.78±0.13†	4.08±0.10†§
Fractional shortening, %	35.3±0.8	37.0±1.1	13.1±0.6†	16.9±0.6†§
Hemodynamic data				
n	15	14	21	26
Heart rate, bpm	447±14	455±14	453±9	466±7
Mean aortic pressure, mm Hg	83±3	78±2	76±2	77±3
LVEDP, mm Hg	2.7±0.5	2.5±0.3	11.4±1.5†	7.6±1.0*‡
Organ weight data				
n	15	14	21	26
Body wt, g	26.9±0.5	27.0±0.8	27.0±0.3	26.4±0.4
LV wt/body wt, mg/g	3.2±0.1	3.0±0.1	4.6±0.3†	4.4±0.1†
Lung wt/body wt, mg/g	5.0±0.1	5.2±0.1	7.6±0.5†	6.4±0.3†‡
Pleural effusion, %	0	0	43	15‡

EDD indicates end-diastolic diameter; ESD, end-systolic diameter; and wt, weight. Values are mean±SEM.

*P<0.05, †P<0.01 vs WT+Sham. ‡P<0.05, §P<0.01 vs WT+MI.

cluding SOD, GSHPx, and catalase activities, were not altered in the TG hearts (Table 1), indicating no effects of Prx-3 overexpression on other antioxidant enzymes. Second, the changes in antioxidants after MI were assessed. Prx-3 protein levels were significantly higher in TG+MI than in WT+MI (Figure 1A) mice. The activities of other antioxidant enzymes were not altered in WT+MI or TG+MI compared with WT+sham animals (Table 1).

The cytoplasmic marker GAPDH was detected exclusively in the cytoplasmic but not in the mitochondrial fraction, whereas COX subunit I was detected preferentially in the mitochondrial but not in the cytoplasmic fraction. This substantiates the integrity of our cellular fractions. Importantly, Prx-3 was detected only in the mitochondrial fraction but not in the cytoplasmic fraction, further confirming that Prx-3 was localized exclusively in the mitochondria (Figure 1B). In addition, immunohistochemical studies showed a homogeneous Prx-3 distribution in cardiac myocytes that colocalized with the mouse mitochondria (Figure 1C). Prx-3 staining showed a relatively spotty pattern. These results further confirm that the rat Prx-3 transgene is not expressed in the cytoplasm within the mouse heart. Mitochondrial TBARS measured in the noninfarcted LV were significantly greater in WT+MI compared with sham animals and were significantly lower in the TG+MI group (Figure 2).

Survival

There were no deaths in the sham-operated groups. Early operative mortality (within 6 hours) was comparable between WT+MI and TG+MI animals (15% versus 7%; P=NS). The survival rate up to 4 weeks tended to be higher in TG+MI compared with WT+MI mice, but this difference did not reach statistical significance (P=0.06 by log-rank test; Figure 3A). Death was suspected to be attributable to heart failure and/or arrhythmia. Five WT+MI (15%) and 2 TG+MI (5%) mice died of LV rupture (P=NS).

Infarct Size

Infarct size as determined by morphometric analysis 28 days after MI was comparable (55±1% versus 56±1%; P=0.83) between WT+MI (n=6) and TG+MI (n=6) groups. To further confirm that overexpression of Prx-3 did not alter infarct size, both the area at risk and infarct area were

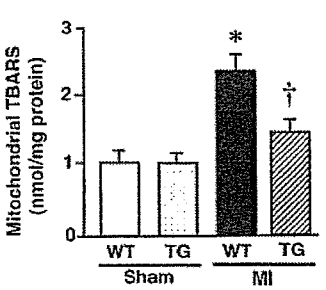

Figure 2. Mitochondrial TBARS in 4 experimental groups of animals (n=8 each). Values are mean±SEM. *P<0.05 for difference from the WT+sham value. †P<0.05 for difference from the WT+MI value.

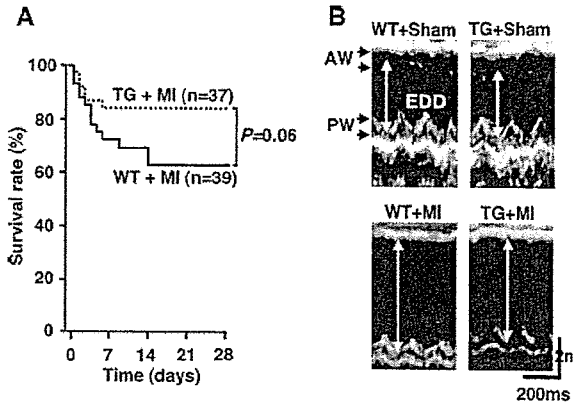

Figure 3. A, Kaplan-Meier survival analysis. Percentages of surviving WT+MI (n=39) and TG+MI (n=37) mice were plotted. Between-group difference was tested by the log-rank test. B, M-mode echocardiograms obtained from WT+sham, TG+sham, WT+MI, and TG+MI mice. AW indicates anterior wall; PW, posterior wall; and EDD, end-diastolic diameter.

measured in mice 24 hours after coronary artery ligation. Percentages of the LV at risk (risk area/LV, 51±3% versus 52±2%; $P=0.89$) and infarct size (infarct/risk area, 79±1% versus 78±1%; $P=0.13$) were also comparable between WT+MI (n=5) and TG+MI (n=5) animals.

Echocardiography and Hemodynamics

The echocardiographic and hemodynamic data of surviving mice at 28 days are shown in Figure 3B and Table 1. LV diameters were significantly larger in WT+MI mice with respect to WT+sham animals. TG+MI mice displayed less LV cavity dilatation and greater fractional shortening than did WT+MI mice. There was no significant difference in heart rate or aortic blood pressure among the 4 groups of mice. LV end-diastolic pressure (LVEDP) was higher in WT+MI than in WT+sham animals, but this increase was significantly attenuated in TG+MI mice.

Organ Weights and Histomorphometry

Coincident with an increased LVEDP, lung weight/body weight was larger in WT+MI mice, and this increase was attenuated in TG+MI mice (Table 1). The prevalence of pleural effusion was also lower in TG+MI than in WT+MI groups. Histomorphometric analysis of noninfarcted LV sections showed that myocyte cross-sectional area was greater in WT+MI mice but was significantly attenuated in TG+MI mice (Figure 4). Collagen volume fraction was greater in WT+MI mice, but this change was inhibited in TG+MI mice (Figure 4).

Myocardial Apoptosis

There were rare TUNEL-positive nuclei in sham-operated mice. The number of TUNEL-positive myocytes in the noninfarcted LV was larger in WT+MI mice but was significantly smaller in TG+MI animals (Figure 5A). In addition, the intensity of the DNA ladder indicated that apoptosis in TG+MI animals was decreased compared with that in WT+MI mice (Figure 5B).

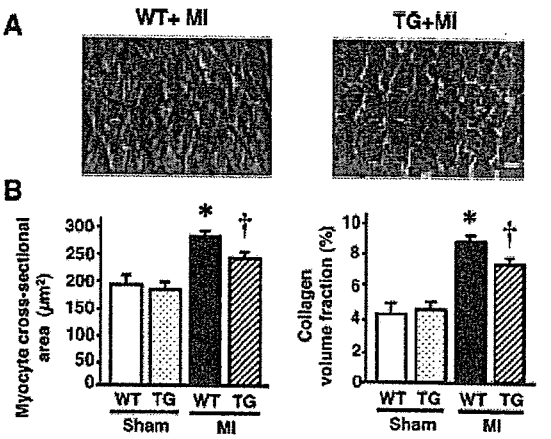

Figure 4. A, Photomicrographs of Masson trichrome–stained LV cross sections obtained from WT+MI and TG+MI mice. Scale bar=10 μm. B, Myocyte cross-sectional area and collagen volume fraction in WT+sham (n=5), TG+sham (n=5), WT+MI (n=8), and TG+MI (n=8) mice. Values are mean±SEM. *$P<0.05$ for difference from the WT+sham value. †$P<0.05$ for difference from the WT+MI value.

mtDNA and Mitochondrial Complex Enzymes Activity

Consistent with our previous studies,[4] mtDNA copy number in the noninfarcted LV from WT+MI animals showed a 36% decrease ($P<0.05$) compared with that in sham-operated mice, which was significantly prevented and was preserved at normal levels in TG+MI animals (Figure 6).

To determine the effects of mtDNA alterations on mitochondrial function, we next measured the mitochondrial electron transport chain complex enzyme activities. The enzymatic activities of complexes I, III, and IV were significantly lower in the noninfarcted LV from WT+MI than in those from WT+sham animals (Table 2). Most important, no such decrease was observed in TG+MI mice. The enzymatic activity of complex II, exclusively encoded by nuclear DNA, was not altered in either group. These results indicate that mtDNA copy number and mitochondrial complex enzymatic activities are downregulated in the post-MI heart and that Prx-3 gene overexpression efficiently counteracts these mitochondrial deficiencies.

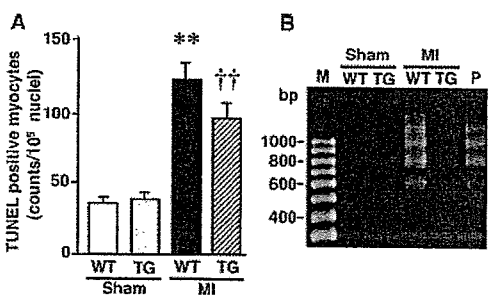

Figure 5. A, Numbers of TUNEL-positive myocytes in the noninfarcted LV from WT+sham, TG+sham, WT+MI, and TG+MI mice (n=5 each). Values are mean±SEM. **$P<0.01$ for the difference from the WT+sham value. ††$P<0.01$ for the difference from the WT+MI value. B, DNA ladder indicative of apoptosis in the genomic DNA from the LV. M indicates marker; P, positive control.

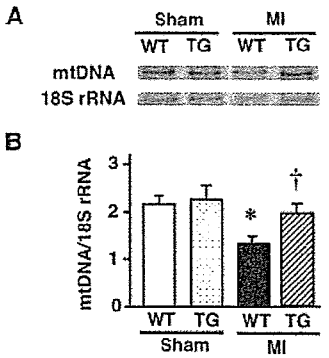

Figure 6. A, Southern blot analysis of mtDNA copy number in total DNA extracts from the hearts from WT+sham, TG+sham, WT+MI, and TG+MI mice. Top bands show signals from the mtDNA fragments, and bottom bands show signals from the nuclear DNA fragments containing the 18S rRNA gene. B, Summary data for a Southern blot analysis of mtDNA copy number in 4 groups of animals (n=8 each). Data were obtained by densitometric quantification of the Southern blots, such as shown in A. Values are expressed as the ratio to WT+sham values and mean±SEM. *$P<0.05$ for the difference from the WT+sham value. †$P<0.05$ for the difference from the WT+MI value.

Plasma TBARS

Plasma TBARS were comparable between WT+MI and TG+MI mice (0.46±0.04 versus 0.54±0.05 μmol/g protein; P=NS).

Discussion

The present study provides the first direct evidence that overexpression of mitochondrial antioxidant Prx-3 protects the heart against post-MI remodeling and failure in mice. It reduced LV cavity dilatation and dysfunction, as well as myocyte hypertrophy, interstitial fibrosis, and apoptosis of the noninfarcted myocardium. These beneficial effects of *Prx-3* gene overexpression were associated with an attenuation of mitochondrial oxidative stress, mtDNA decline, and dysfunction. They were not due to its MI size-sparing effect but occurred secondary to more adaptive remodeling.

Mitochondria are the predominant source of ROS in the failing myocardium.[1] Most of the $\cdot O_2^-$ generated by the mitochondria is vectorially released into the mitochondrial matrix. $\cdot O_2^-$ impairs mitochondrial function by oxidizing the Fe-S centers of complex enzymes. In addition, $\cdot O_2^-$ is converted to peroxynitrite, an extremely powerful oxidant, as a result of its reaction with NO produced by mitochondrial NO synthase. $\cdot O_2^-$ is also converted to H_2O_2 by a specific intramitochondrial Mn-SOD. Although Mn-SOD relieves mitochondrial oxidative stress caused by $\cdot O_2^-$, it generates H_2O_2 and therefore, further enhances a different type of oxidative stress. H_2O_2 can damage cellular macromolecules such as proteins, lipids, and nucleic acids, especially after its conversion to ·OH. Moreover, these increased ROS in the mitochondria were associated with a decreased mtDNA copy number and reduced oxidative capacity owing to low complex enzyme activities.[4] Therefore, chronic increases in mitochondrial ROS production cause mtDNA damage and dysfunction, which thus, can lead to a catastrophic cycle of further oxidative stress and ultimate cellular injury.[5] This deleterious process may play an important role in the development and progression of myocardial remodeling and failure.[4] Based on these results, mitochondrial antioxidants are expected to be the first line-of-defense mechanism against ROS generation in the mitochondria and ROS-mediated mitochondrial injury and thus, may protect the heart from adverse remodeling and failure.

Prx-3, which was formerly known as SP-22, or MER5, is currently identified as a mitochondrial member of the novel antioxidant proteins designated as Prxs.[15] Among 6 known mammalian Prxs, Prx-1 to -4 require the small redox protein thioredoxin (Trx) as an electron donor to remove H_2O_2, whereas Prx-5 and -6 can use other cellular reductants, such as GSH, as their electron donor.[16] Prx-1, -2, and -6 are found in the cytoplasm and nucleus,[7] whereas Prx-3 contains a mitochondrial localization sequence, is found exclusively in the mitochondria, and uses mitochondrial Trx-2 as the electron donor for its peroxidase activity.[17] It functions not only by removing H_2O_2 formed after the SOD-catalyzed dismutation reaction but also by detoxifying peroxynitrite.[6] Therefore, the great efficiency of Prx-3 as an antioxidant shown in the present study may be attributable to the fact that it is located in the mitochondria and can utilize lipid peroxides as well as H_2O_2 for substrates. In fact, overexpression of Prx-3 has been shown to protect thymoma cells from apoptosis induced by hypoxia, a bolus of peroxide, or an anticancer drug.[18] Moreover, Prx-3 overexpression has been reported to protect rat hippocampal neurons from excitotoxic injury.[8] Prx-5 is also associated with the mitochondria in addition to the peroxisomes and nucleus. Recently, increased expression of Prx-5 was found to have protected Chinese hamster ovary cells from mtDNA damage induced by oxidative stress.[19] Therefore, Prx-5 may also exert beneficial effects against mitochondrial oxidative stress in post-MI hearts.

GSHPx also catalyzes the reduction of H_2O_2. In fact, our previous studies demonstrated that overexpression of GSHPx

TABLE 2. Mitochondrial Complex Enzyme Activities

	WT+Sham	TG+Sham	WT+MI	TG+MI
n	7	7	7	7
Complex I, nmol/min per mg protein	282±26	265±38	159±25*	287±16†
Complex II, nmol/min per mg protein	770±70	718±93	711±85	726±128
Complex III, nmol/min per mg protein	505±11	470±31	367±20*	451±21†
Complex IV, nmol/min per mg protein	1223±37	1175±34	744±68*	939±54†

Values are mean±SEM.
*$P<0.05$ vs WT+sham; †$P<0.05$ vs WT+MI.